京都大学学術情報リポジトリ
KURENAI 紅
Kyoto University Research Information Repository

京都大学
KYOTO UNIVERSITY

Title	A sequence of a plinian eruption preceded by dome destruction at Kelud volcano, Indonesia, on February 13, 2014, revealed from tephra fallout and pyroclastic density current deposits
Author(s)	Maeno, Fukashi; Nakada, Setsuya; Yoshimoto, Mitsuhiro; Shimano, Taketo; Hokanishi, Natsumi; Zaennudin, Akhmad; Iguchi, Masato
Citation	Journal of Volcanology and Geothermal Research (2017)
Issue Date	2017-03-07
URL	http://hdl.handle.net/2433/241765
Right	© 2018 Elsevier B.V. This is an open access article under the CC BY license (http://creativecommons.org/licenses/by/4.0/).
Type	Journal Article
Textversion	publisher

Kyoto University

Journal of Volcanology and Geothermal Research xxx (2018) xxx–xxx

Contents lists available at ScienceDirect

Journal of Volcanology and Geothermal Research

journal homepage: www.elsevier.com/locate/jvolgeores

A sequence of a plinian eruption preceded by dome destruction at Kelud volcano, Indonesia, on February 13, 2014, revealed from tephra fallout and pyroclastic density current deposits

Fukashi Maeno [a,*], Setsuya Nakada [a], Mitsuhiro Yoshimoto [b], Taketo Shimano [c], Natsumi Hokanishi [a], Akhmad Zaennudin [d], Masato Iguchi [e]

[a] Earthquake Research Institute, University of Tokyo, 1-1-1 Yayoi, Bunkyo-ku, Tokyo 113-0032, Japan
[b] Mount Fuji Research Institute, Yamanashi Prefectural Government, 5597-1 Kenmarubi, Kamiyoshida, Fuji-yoshida, Yamanashi 403-0005, Japan
[c] Graduate School of Environment and Disaster Research, Tokoha University, Obuchi 325, Fuji City, Shizuoka 417-0801, Japan
[d] Center for Volcanology and Geological Hazard Mitigation, Bandung, Indonesia
[e] Sakurajima Volcano Research Center, Disaster Prevention Research Institute, Kyoto University, 1722-19 Sakurajima-Yokoyama-cho, Kagoshima 891-1419, Japan

ARTICLE INFO

Article history:
Received 19 July 2016
Received in revised form 27 January 2017
Accepted 1 March 2017
Available online xxxx

Keywords:
Plinian
Pyroclastic density current
Blown-down tree
Lava dome
Kelud volcano

ABSTRACT

A plinian-style eruption with a radially spreading umbrella cloud occurred on February 13, 2014, at Kelud volcano, Indonesia. We present the sequence of this plinian event based on a geological survey of the eruption products and analysis of satellite images. The eruptive deposits were divided into four major depositional units (Units A, B, C, and D) and used to determine the sequence of events. The plinian phase was preceded by partial destruction of the existing lava dome and generation of high-energy pyroclastic density currents (PDCs) mainly toward the NE that produced a series of depositional subunits (Units A_{0-2}) and blown-down trees (stage 1). In the main phase of the plinian eruption, tephra fallout (Unit B) was widely distributed over East Java (stage 2). The winds above the volcano significantly affected the tephra dispersal process. In stage 3, the plinian column collapsed, generating dense PDCs that flowed down the volcano valleys, producing pumiceous lobate deposits (Unit C). The declining phase of the eruption produced fine-rich fallout tephra layers (Unit D_{1-2}) from low-level eruption plumes and/or ash lofted from PDCs. The eruption sequence constructed from field observations is supported by geophysical observations. The deposit features and componentry suggest that newly ascended magma triggered the destruction of the lava dome and the generation of high-energy PDCs, and during the subsequent climactic phase the dome was completely destroyed. We estimate a total erupted volume of 0.25–0.50 km^3 (bulk deposit volume, 0.14–0.28 km^3 in dense rock equivalent) and a mass eruption rate of $6.5 \pm 2.8 \times 10^7$ kg/s, with a volcanic explosivity index of 4. The eruption sequence and physical parameters of the 2014 eruption will help assess future volcanic activity and hazards at Kelud volcano.

© 2018 Elsevier B.V. This is an open access article under the CC BY license (http://creativecommons.org/licenses/by/4.0/).

1. Introduction

Plinian eruptions, characterized by sustained, explosive magma discharge, are among the most powerful eruption styles of andesitic to rhyolitic volcanoes. These eruptions generate a buoyant eruption column to a height of ~20–40 km or more (e.g., Carey and Sigurdsson, 1989; Cioni et al., 2015), resulting in widespread tephra fallout. They are often accompanied by the generation of pyroclastic density currents (PDCs), which are an extremely hazardous volcanic phenomenon at active volcanoes close to populated areas (e.g., El Chichon, Sigurdsson et al., 1987; Vesuvius, Cioni et al., 1992; Kelud, Bourdier et al., 1997; and Colima, Saucedo et al., 2010). Unveiling the eruption process in detail and estimating the physical parameters, such as volume and discharge rate, for each eruptive event is thus important to understand the nature and dynamics of plinian eruptions, and the evolution of the underlying magmatic systems. Examining the products from a recent well-observed eruption using satellite and geophysical monitoring may also help to understand the eruptive style of the volcano and characterize the predicted patterns of future activity for volcanic hazard assessment.

The eruption at Kelud volcano, East Java, in 2014 provides an opportunity to study the sequence and physical parameters of a plinian eruption, and to evaluate the associated hazards. We show that this plinian event, which had a radially spreading umbrella cloud, was preceded by the destruction of a lava dome, and accompanied by high-energy PDCs. The sequence of this eruption was similar to past explosive eruptions that were preceded by a lava dome or cryptodome growth, for example, Mount Lamington in 1951 (Taylor, 1958), Bezymianny volcano

* Corresponding author.
E-mail address: fmaeno@eri.u-tokyo.ac.jp (F. Maeno).

http://dx.doi.org/10.1016/j.jvolgeores.2017.03.002
0377-0273/© 2018 Elsevier B.V. This is an open access article under the CC BY license (http://creativecommons.org/licenses/by/4.0/).

Please cite this article as: Maeno, F., et al., A sequence of a plinian eruption preceded by dome destruction at Kelud volcano, Indonesia, on February 13, 2014, revealed from tep..., J. Volcanol. Geotherm. Res. (2018), http://dx.doi.org/10.1016/j.jvolgeores.2017.03.002

in 1956 (Belousov, 1996), Mount St. Helens in 1980 (Hoblitt et al., 1981), Mount Pinatubo in 1991 (Hoblitt et al., 1996), and Merapi volcano in 2010 (Komorowski et al., 2013), or eruptions accompanied by high-energy PDCs in the vent-opening phase, e.g., Mount Pelee in 1902 (Boudon and Lajoie, 1989) and Chaiten volcano in 2008 (Major et al., 2013). The lava dome at Kelud was formed in the last eruption in 2007–2008 (De Belizal et al., 2012; Jeffery et al., 2013). Therefore, in addition to understanding the basic features of this plinian eruption, it is important to examine the factors that control dome destruction and the generation of the high-energy PDCs after six years of dormancy. We present results of field observations of the eruption products from the 2014 Kelud eruption, analysis of satellite images of the eruption plume, and surface features of the volcanic edifice before and after eruption. The deposit data obtained by our field survey immediately after the eruption were used to estimate the physical parameters of the eruption, and to constrain the generation and emplacement processes of the PDCs preceding and following the plinian phase. This work also contributes to understanding the hazards posed by Kelud volcano.

2. Outline of Kelud volcano and the 2014 eruption

Kelud volcano, East Java, is one of the most active and hazardous andesitic stratovolcanoes in Indonesia, having caused >15,000 casualties through its historic eruptions. The volcano has erupted repeatedly since at least 1000 CE, with various eruption styles: plinian, dome-forming, and phreatomagmatic eruptions (Siebert et al., 2011). The 20th century eruptions were plinian in style, accompanied by PDCs and extensive fallout deposition (1901, 1919, 1951, 1966, and 1990) or dome-building (1920, and 2007–2008). All the plinian eruptions in the 20th century had a recorded volcanic explosivity index (VEI; Newhall and Self, 1982) of 4. The major disasters were caused by devastating lahars associated with a breakout of the summit crater lake during or after the eruption.

The most recent eruption before 2014 was an effusive dome-forming eruption in 2007–2008. The eruption began in early November 2007, following an increase in seismic activity in September 2007, and lasted approximately seven months. The eruption created a new lava dome within the summit crater that protruded from and eventually displaced the existing crater lake (De Belizal et al., 2012; Jeffery et al., 2013). By May 2008, the lava dome stopped growing, having reached an estimated size of ~260 m in height, ~400 m in width at its base, and 3.5×10^7 m^3 in volume (Siebert et al., 2011).

A 6-year period of quiescence began in 2008. Then, in January 2014, the number of volcanic earthquakes increased. Their number and magnitude further increased from February 2, 2014, and continued to rise until the eruption on February 13, 2014. At 15:46 UTC (22:46 local time) on February 13, 2014, the seismic signal recorded at the near-crater station abruptly disappeared, indicating the onset of the explosion event. Observers in the Kelud Volcano Observatory (POS), ~6 km west of the summit crater, reported that a real-time camera on the crater rim captured ballistic ejecta as its final image at almost the same time (~22:45). Therefore, the erupting materials must have hit the seismic stations at this time. The explosion was followed by the main plinian eruption.

A satellite first detected the umbrella cloud at 16:09 UTC; the CALIOP (Cloud-Aerosol Lidar with Orthogonal Polarization) measured its strongest signal at altitudes around 17–18 km, with the top of the umbrella cloud at 18–19 km (Kristiansen et al., 2015). The eruption cloud spread radially, and its diameter exceeded 200 km by 17:32 UTC (Fig. 1). The circular eruption cloud then drifted westward across the island of Java, while slightly expanding in both the down- and cross-wind directions and changing to an ellipse or similar shape, reflecting the asymmetric dimensions of the umbrella. Satellite images indicate that the vigorous plinian plume continued for ~2.5 h, but remote seismo-acoustic signals suggest that the eruption plume weakened by 18:00 UTC and the resonant oscillation between the atmosphere and the ground continued for another hour (Caudron et al., 2015; Nakashima et al., 2016). These observations indicate that the most vigorous plinian phase lasted 2–2.5 h. 9 h later, the center of the eruption cloud drifted about 600 km westward over the Indian Ocean. Our field survey and interviews, and eyewitness and media reports (Nakada et al., 2016) indicate that the tephra distribution was generally consistent with the development of the eruption plume (Fig. 2) as seen in satellite images. However, no ashfall was observed in the eastern and southern areas of the Kelud volcano.

3. Surface changes of the volcanic edifice due to the 2014 eruption

In addition to our field survey, we investigated the surface changes of the volcanic edifice of Kelud volcano using satellite images that were taken before and after the eruption. The pre-eruption surface features were taken from GoogleEarth images (taken by Quickbird, a high-resolution commercial earth observation satellite owned by DigitalGlobe, US) on August 23–24, 2012, and August 9, 2013. For the post-eruption surface features, we used WorldView-2 images taken on May 19, 2014, with a spatial resolution of ~50 cm. The overall surface features after the 2014 eruption are shown in Fig. 3, where the whitish-gray areas indicate the major zones disturbed by PDCs. In Fig. 4 we

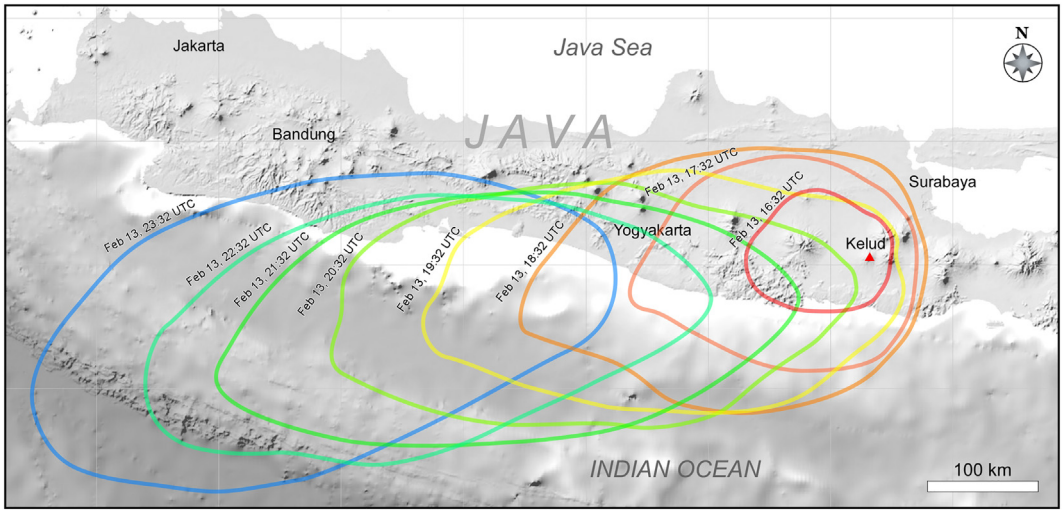

Fig. 1. Location map with the sequence of plume development of the eruption at Kelud volcano, Indonesia, on February 13, 2014. Color lines show the scope of the eruption plume at one-hour intervals from 16:32 UTC (red circle) to 23:32 UTC (blue one). The plume traces were produced based on MTSAT-2 satellite images obtained by the Japan Meteorological Agency.

Please cite this article as: Maeno, F., et al., A sequence of a plinian eruption preceded by dome destruction at Kelud volcano, Indonesia, on February 13, 2014, revealed from tep..., J. Volcanol. Geotherm. Res. (2018), http://dx.doi.org/10.1016/j.jvolgeores.2017.03.002

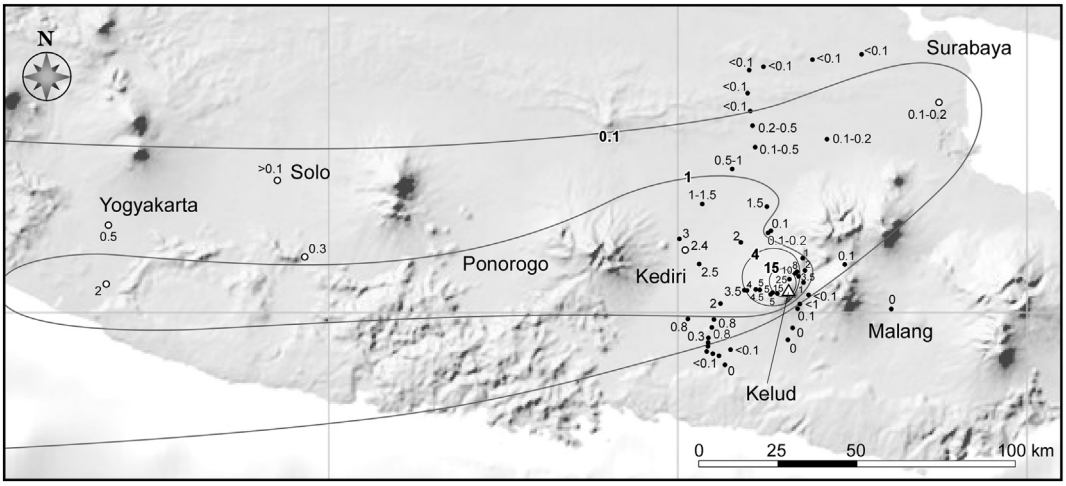

Fig. 2. Tephra thickness data and isopach map of the fallout deposit from the 2014 Kelud eruption. Closed circles are data from our geological survey. Open circles are data from eyewitness reports. Contours represent thicknesses of 15, 4, 1, and 0.1 cm. Units: cm.

Fig. 3. Optical satellite image of Kelud volcano after the 2014 eruption and locality map. The satellite image was taken by WorldView-2, on May 19, 2014. Numbers indicate sites where field surveys were carried out. White squares outline areas enlarged in Fig. 4.

Please cite this article as: Maeno, F., et al., A sequence of a plinian eruption preceded by dome destruction at Kelud volcano, Indonesia, on February 13, 2014, revealed from tep..., J. Volcanol. Geotherm. Res. (2018), http://dx.doi.org/10.1016/j.jvolgeores.2017.03.002

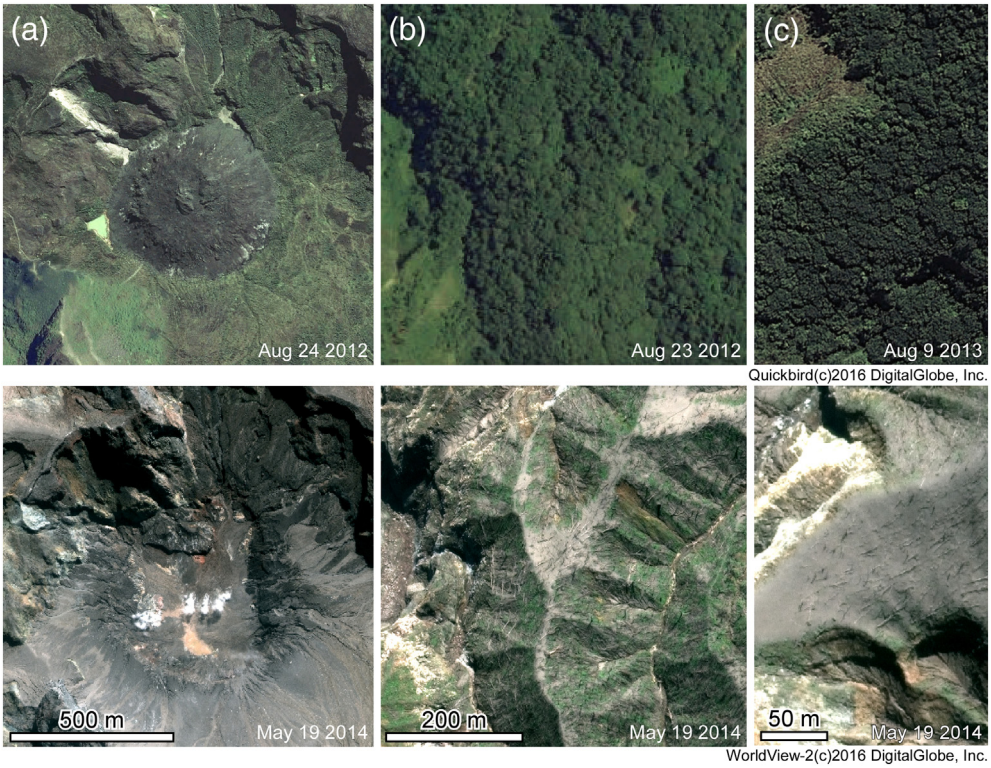

Fig. 4. Comparison of surface features pre- and post-2014 Kelud eruption. Upper panels show the pre-eruption, vegetated surface of selected areas (indicated in Fig. 3), and bottom ones show the same areas after the eruption. (a) Inside the summit crater of Kelud volcano. Before the 2014 eruption, a lava dome produced in the 2007–2008 eruption existed, but it was completely destroyed during the 2014 eruption. In its place remains an irregular-shaped depression. Vegetation was also blown off completely. (b) Area around site #334 on the NE edifice, ~3 km from the rim of the summit crater, where a field survey was carried out. (c) Area on the eastern edifice of the volcano, ~2 km from the rim of the summit crater, where almost all the vegetation was blown off. The fallen trees lie along the ENE–WSW direction.

compare the surface features of the pre- and post-2014 eruptions in selected areas. Before the 2014 eruption, most of the surface of Kelud volcano, including the summit crater, was vegetated. A lava dome that was formed in 2007–2008 occupied the summit crater (Fig. 4a) before the eruption, but was completely destroyed during the eruption. In its place, an irregularly shaped depression with a diameter of ~500 m (the 2014 eruption crater) was formed. On the northeastern edifice around site #334, ~3 km from the rim of the summit crater where a field survey was carried out, almost all the trees a few tens of meters in height were blown down along the valley (Fig. 4b). On the eastern edifice, ~2 km from the rim of the summit crater, many blown-down trees were observed trending WSW–ENE (Fig. 4c). This direction is parallel to the strike lines along the valley slope, indicating that the flows travelled along the valleys. The vegetation at this site was completely blown away. Similar features were observed in many places along the valleys surrounding the summit crater, but the area with blown-down trees and vegetation, and an eroded ground surface (whitish or light gray color in Fig. 3) was more extensive northeast of the volcano. The major surface features and deposits caused by the eruption are summarized in Fig. 5. The directions in which the blown-down trees were oriented, indicated by small arrows, were determined based on satellite images and field observations.

4. Stratigraphy and description of eruptive deposits

The stratigraphy of the products from the 2014 eruption was compiled based on field surveys carried out in and around Kelud volcano in March and November 2014. In this section, we show the stratigraphic relationship of the eruption products and describe the deposits. The interpretation of each deposit is provided in Section 7.1. The eruption deposits can be divided into four major depositional units (Units A, B, C, and D), corresponding to the main phases of the 2014 event. Representative outcrop locations are shown in Figs. 2 and 3. The stratigraphic columns of the deposits at selected locations are shown in Fig. 6.

Unit A consists of the lowest part of the deposits and is divided into three subunits (Units A_0, A_1, and A_2). Unit A was found only on the NE ridges, extending at least 4.3 km from the rim of the summit crater. The thickness of the unit decreases from ~20 cm (at site #334) to 7 cm (at site #330). The overall thickness variation through the NE area is not known, but the unit appears to cover the ground surface as a thin deposit. Unit A_1 is the main thick part of the deposit, while Units A_0 and A_2 are the base and top layers, respectively, representing thin ash-rich, poorly sorted deposits a few mm to 2-cm thick (Figs. 6, 7). Units A_0–A_2 are yellowish to brownish gray in color, and contain pumice (5–20 wt%), fresh and altered lithics (from the 2007–2008 lava), and crystal and organic fragments (also see Section 6 for components). Unit A_1 is characterized by massive, moderately sorted facies with lapilli and ash as the dominant components. It contains coarse grains, composed of fresh or altered angular lava fragments (<14 cm in diameter at site #334, and <2 cm at site #330) and subangular pumice (<10 cm in diameter at site #334, and <3 cm at site #330), as well as uncharred branches and leaves, or partially charred wood and leaf fragments (Fig. 7). The grading structures of the deposits are unclear or lacking, and there is no internal stratification in the deposits.

The area covered by the blown-down trees along the valleys and ridges in the northeastern area corresponds to the same stratigraphic level as Unit A. The area of blown-down trees and vegetation extends over ~12 km^2 with a maximum distance of ~6.8 km from the vent. In particular, in the NE area within 1–2 km from the rim of the summit crater, the surface of the slopes along the valleys is strongly eroded and has no vegetation (Figs. 3, 5). Along the margin of the damaged area, only some leaves and branches were blown off. Some key features observed on the ground are shown in Fig. 8. Around site #334 on the NE ridge, trees were blown down, cut, bent, or uprooted. They all lie in the

Please cite this article as: Maeno, F., et al., A sequence of a plinian eruption preceded by dome destruction at Kelud volcano, Indonesia, on February 13, 2014, revealed from tep..., J. Volcanol. Geotherm. Res. (2018), http://dx.doi.org/10.1016/j.jvolgeores.2017.03.002

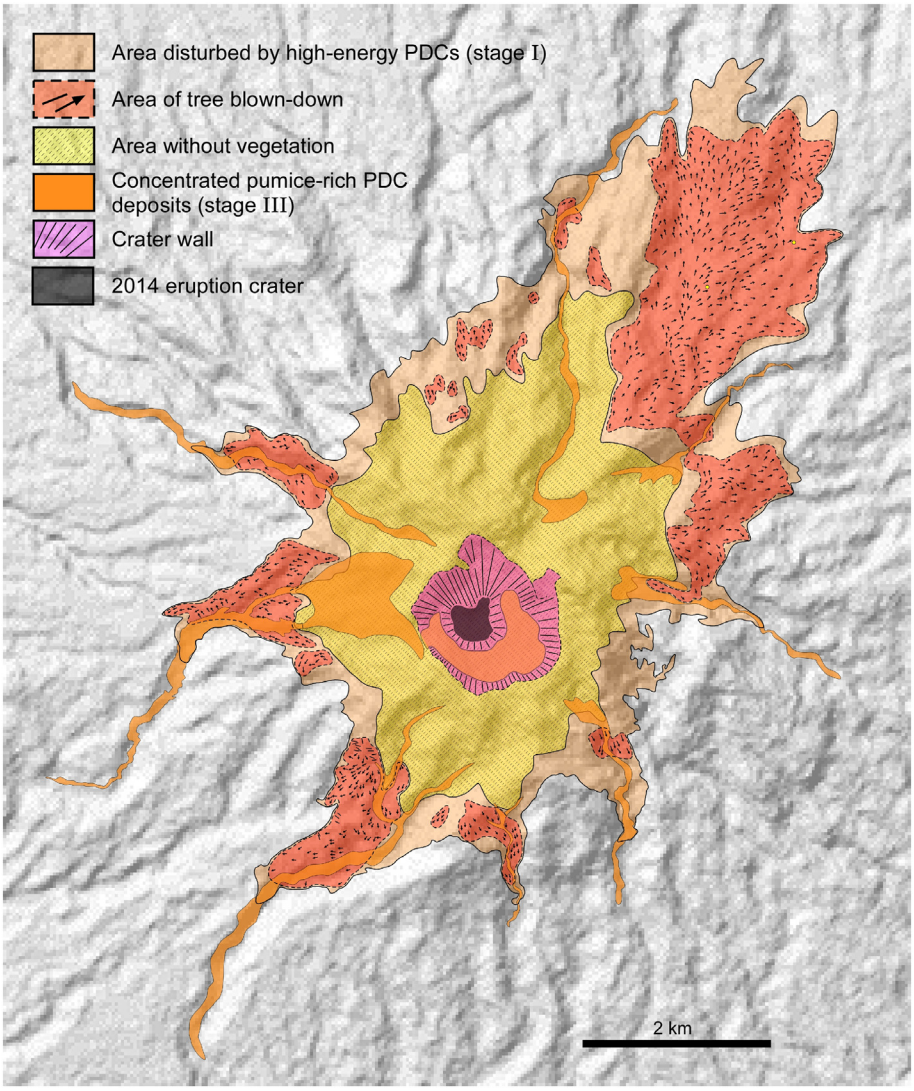

Fig. 5. Map showing the area affected by the eruption, and distribution of the PDC deposits. Small arrows indicate the PDC flow direction, estimated from the direction of the fallen trees, based on satellite images and field observations. The map is based on the WorldView-2 image on May 19, 2014 (Fig. 3), three months after the eruption. The background is a shaded-relief topographic map of Kelud volcano produced from the Global Digital Elevation Model issued by Jet Propulsion Laboratory, NASA.

same direction (to the NE at this location, Fig. 3; Fig. 8a, b). Well-sorted fallout pumice covers the trees (Fig. 8c, d). Tree trunks facing the summit are also severely damaged by angular lithic fragments ejected from the volcano (Fig. 8e, f). Blown-down trees were also observed on the western and southern sides of the volcano; however, most of them belong to a later stratigraphic stage. Charred trees were often observed in these areas, while the trees in the NE area were uncharred.

Unit B consists of the middle, most voluminous part of the deposits. It is widely distributed around the volcano and has two major axes extending W and NE (Figs. 2, 6, 7). The deposit is characterized by massive, moderately sorted and mostly fine-poor facies, and the sorting improves with distance. The deposit consists mainly of angular pumice lapilli, but also fresh and altered lithic material, and shows a clast-supported structure (Fig. 9a, b). The maximum clast size for both pumice and lithic material is a few tens of cm in diameter at ~500 m from the vent, ~10–15 cm at ~2 km, and decreasing to <1 cm around Kediri, 30 km west of the volcano. Unit B generally shows reverse grading near the base and normal grading toward the top in the proximal area. On the northern side, the grain size decreases to fine ash at the top. However, on the western side, the normal grading at the top is unclear. The overall grading structures become unclear with distance. In areas NE of the volcano, Unit B directly covers Unit A, or the blown-down trees (Fig. 8). In the proximal area on the western side, Unit B directly overlies the pre-eruption ground surface (an old lava or a paved road), or ballistic ejecta with impact craters from the initial stage of eruption. The thickness of the unit decreases from ~8 cm at Ngantur (Fig. 9a) to a few cm around Kediri. In the northern area toward Surabaya, the thickness of the ash deposit decreases to a few mm (Fig. 2). At Yogyakarta ~200 km away, the observed thickness of the ash deposit was ~2 cm.

Unit C consists of a series of pumiceous lobate deposits lying mainly in the valleys. This unit can be divided into several subunits that correspond to multiple lobes. The thickness of each subunit (lobe) varies depending on the locality, reaching a maximum of ~3 m or more. The deposit is characterized by gray to pinkish, massive, poorly sorted fine-grained facies, containing abundant pumice and lava blocks up to 20 cm in diameter. In the western and southern valleys, coarse subrounded to rounded pumice clasts up to 50 cm in diameter are generally concentrated on the surface and along the margin of the lobate deposits (e.g., site #224, Figs. 6, 9c, d). Fragments of charred wood can also be observed. Numerous degassing pipes are also observed in the deposit. In some locations, the massive unit includes relatively well-sorted ash layers at the base and top near the source (Fig. 6). Along the southern and western valleys, the deposit is distributed up to 3–

Please cite this article as: Maeno, F., et al., A sequence of a plinian eruption preceded by dome destruction at Kelud volcano, Indonesia, on February 13, 2014, revealed from tep..., J. Volcanol. Geotherm. Res. (2018), http://dx.doi.org/10.1016/j.jvolgeores.2017.03.002

ARTICLE IN PRESS

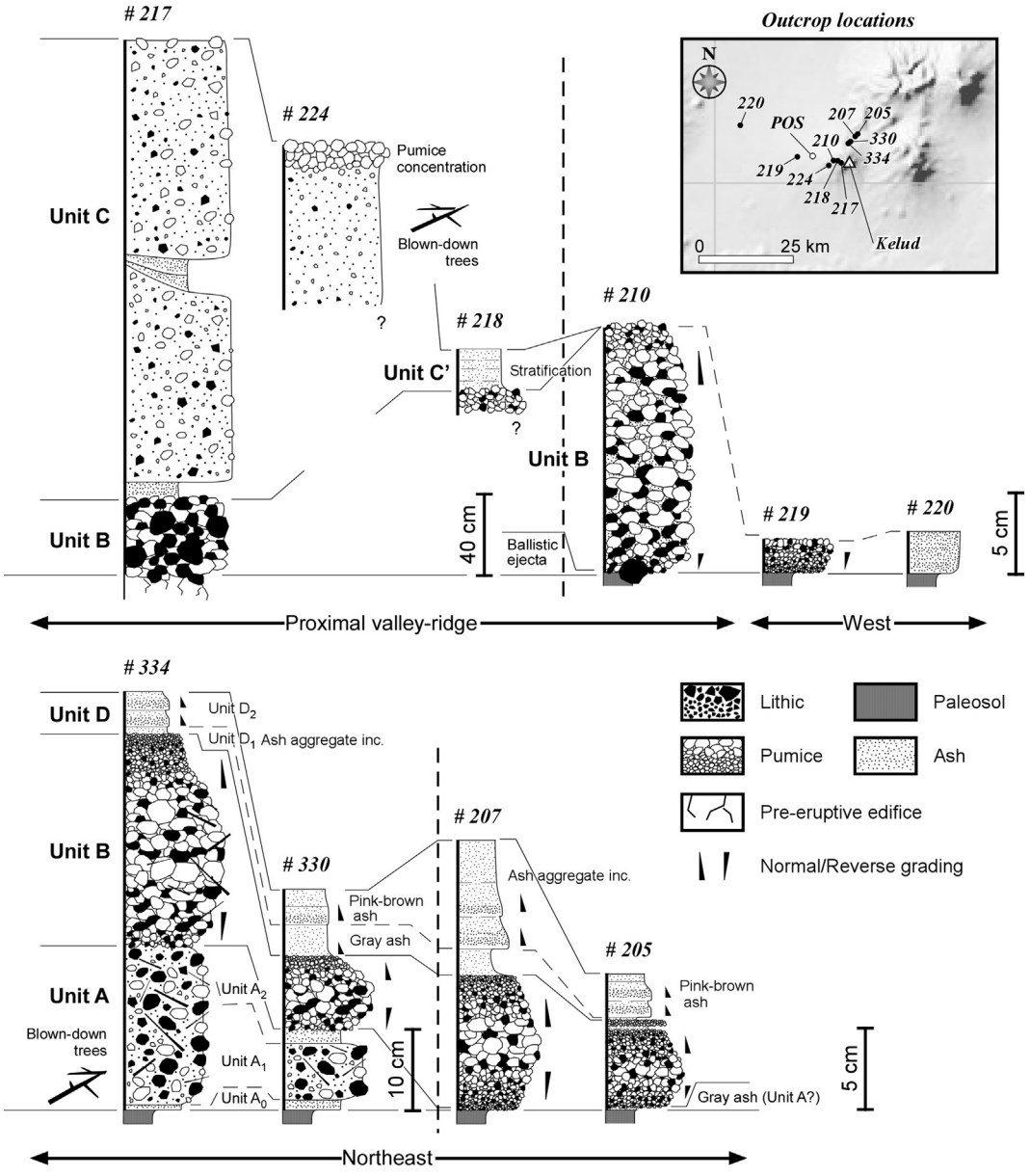

Fig. 6. Stratigraphic columns of eruption deposits at representative locations around Kelud volcano. Upper right panel shows outcrop locations.

5 km from the rim of the summit crater. We were not able to survey the main deposits on the northern and eastern sides, but the approximate distribution can be inferred based on satellite images. In the proximal area (at site #217), the stratigraphic relationship between Units B and C is clearly identified (Fig. 9b). Most of the sections with blown-down trees in the western and southern areas belong to the same stratigraphic level as Unit C because there was no later deposition in these areas. Some of the damaged parts of the blown-down trees are charred (Fig. 9e). In the western valley, 2.5 km from the rim of the summit crater, explosion craters were observed on the surface of Unit C. This is consistent with observations (at POS) that a number of secondary explosions occurred in the valleys after the eruption. On the ridge along the western valley, gray poorly sorted ash-rich layers with weak stratification occasionally cover the better-sorted Unit B pumice deposit (e.g., site #218, Figs. 6, 9f). These layers correspond to the same stratigraphic level as Unit C, but are thinner and finer. We defined this deposit as Unit C′.

Unit D consists of the upper part of the deposits and is divided into two subunits (Units D_1 and D_2). Unit D_1 is a gray fine ash layer on top of Unit B, and Unit D_2 consists of pink-brown, stratified fine ash layers. These ash layers are only observed on the northeastern side (sites #334, 207, and 205; Figs. 6, 7, 9). Each layer is normally graded and has some ash-accretion textures. This unit corresponds to the same or later stratigraphic level as Units C and C′.

The summit crater is filled with a thick pyroclastic deposit approximately 15–20 m thick (Fig. 9g). This deposit overlies talus deposits of the pre-existing lava dome near the 2014 eruption crater. The deposit may be divided into several subunits, but it is difficult to correlate these units to the major eruption units observed outside the summit crater. The lower part of the deposit (3–5 m in thickness) is a massive, relatively well-sorted deposit, and the upper part of the deposit (10 m or more in thickness) is characterized by massive, poorly sorted, and fine-grained facies. The pyroclastic deposit contains large lava blocks (up to 3 m in diameter) derived from the pre-existing lava dome.

5. Composition of erupted magma

The pumice that erupted in 2014 was highly porphyritic basaltic andesite with ~55 vol% of phenocrysts of plagioclase, clinopyroxene, orthopyroxene, and titanomagnetite, all of which also occur as aggregates (clots). The whole-rock composition is 55.0–55.7 wt% in SiO_2,

Please cite this article as: Maeno, F., et al., A sequence of a plinian eruption preceded by dome destruction at Kelud volcano, Indonesia, on February 13, 2014, revealed from tep..., J. Volcanol. Geotherm. Res. (2018), http://dx.doi.org/10.1016/j.jvolgeores.2017.03.002

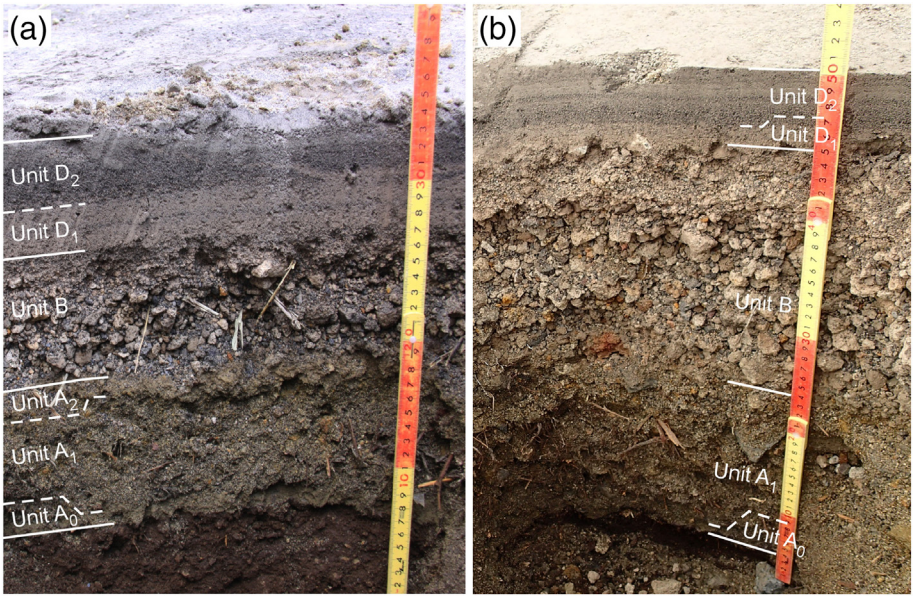

Fig. 7. Eruptive deposit from the 2014 Kelud eruption observed at sites (a) #330 and (b) #334. The deposits are divided into three major units (Units A, B, and D) and subunits for Unit A (A_0, A_1, and A_2) and Unit D (D_1 and D_2). Both photos were taken on November 22, 2014. (For interpretation of the references to color in this figure, the reader is referred to the web version of this article.)

analyzed by an X-ray Fluorescence Spectrometer (ZSX Primus II, Rigaku Co., Ltd., Tokyo, Japan) at the Earthquake Research Institute, University of Tokyo (Supplementary Table A). The matrix glass composition is dacitic to rhyolitic with 69.3–70.3 wt% in SiO_2, analyzed by an Electron Probe Micro-Analyzer (JXA-8800R, JEOL Ltd., Tokyo, Japan) at the Earthquake Research Institute, University of Tokyo (Supplementary Table A). These whole-rock chemical and mineral compositions of the 2014 pumice are similar to those of the lava that erupted in 2007–2008 (Jeffery et al., 2013). However, the textures and glass compositions are different; the pumice is more vesicular and the glass composition is less evolved. The materials that erupted in 2014 include juvenile pumice from this eruption, fresh lithic (dense lava) originating from the 2007–2008 lava dome, and hydrothermally altered lava derived from the 2007–2008 or older eruptions. Particles less than a few mm in diameter include shattered isolated crystals originating from the porphyritic magmas of the 2014 or 2007–2008 eruptions.

6. Grain-size and component variations

Grain-size and component analyses were carried out for representative units from selected locations. The overall grain size characteristics of Units A and B are summarized in the Md_φ-σ_φ plots (Md: median diameter; σ_φ: sorting coefficient, Inman, 1952) (Fig. 10). For all the samples, σ_φ was less than 3φ. Unit B shows typical fallout characteristics, and the sorting improves with distance. Unit A is more poorly sorted than Unit B, and has both fall and flow features. The grain-size histogram for Unit A_1 at site #330 shows a relatively broad distribution with two marked populations (Fig. 11). The coarser population around −2φ consists mostly of pumice and lithic fragments, while the finer population with 2φ is composed mostly of shattered crystals. The proportion of lithic fragments is much higher than that in the other units. The mean size of the crystal fragments in Unit A_1 is finer than that in the fallout tephra (Unit B). The same grain characteristics of Unit A_1 appear at sites #334 and #330, 3.7 km and 5 km NE from the source, respectively. The underlying Unit A_0 is fine grained and poorly sorted, with a relatively broad unimodal grain-size distribution (Fig. 11). The component data of Unit A_0 was obtained only for coarse ash, but it is not significantly different from that of Unit A_1 and also contains juvenile pumice. The grain-size histogram for Unit B at site #330 shows a coarser and unimodal distribution, with a higher proportion of pumice than in Unit A (Fig. 11). It generally contains 40–60 wt% pumice while Unit A has only ~20 wt% pumice.

The grain-size histograms for Unit B vary with distance from the source (Fig. 12). Within 15 km of the source, they show relatively broad distributions with bimodal populations; thus, the bulk of the deposit is not well sorted. However, as shown in Fig. 11, the grain-size distribution appears to be a combination of a coarser population in the pumice clasts and a finer population in the isolated crystals. The sorting of each component is fall-like in nature, becoming better sorted with distance from the source (from 2 to 11 km from the summit crater). Simultaneously, the mean diameter of the pumice decreases from −3φ to −1.5φ, but the size of the isolated crystals is almost constant at 0.5–1.0φ. In the distal area, >20 km from the source, the sorting for the entire deposit at each site improves, and the grain-size histograms show a unimodal distribution with a population of <500 μm (Fig. 12). The maximum clast size of Unit B was also measured in the field and is shown in Fig. 12. A 2-cm-isopleth for pumice clasts covers an area of ~500 km^2 to the west of the volcano.

7. Discussion

7.1. Origin of eruptive deposits

The deposits from the 2014 Kelud eruption can be divided into four major depositional units (Units A–D). In this section, we interpret each depositional unit and discuss their origin to clarify the evolution and dynamics of the eruption.

7.1.1. Unit A

Unit A is distributed on the ridges NE of the crater. The deposits lie on the same stratigraphic level as the blown-down trees that extend at least 12 km^2 to the NE. In particular, the main part of the deposit, Unit A_1, is massive (without internal cross-bedding) and moderately sorted. The broad grain-size distribution lacks fines, with multimodal populations, and organic-rich deposits. The main depositional unit (A_1) underlies a top layer with poorly sorted facies (A_2). Although our field data are limited, all these lines of evidence indicate that the deposits were produced from dilute high-energy PDCs that traveled along topographic lows but also deposited eruptive material on the ridges from tens to a hundred meters high. The Md_φ-σ_φ relationship

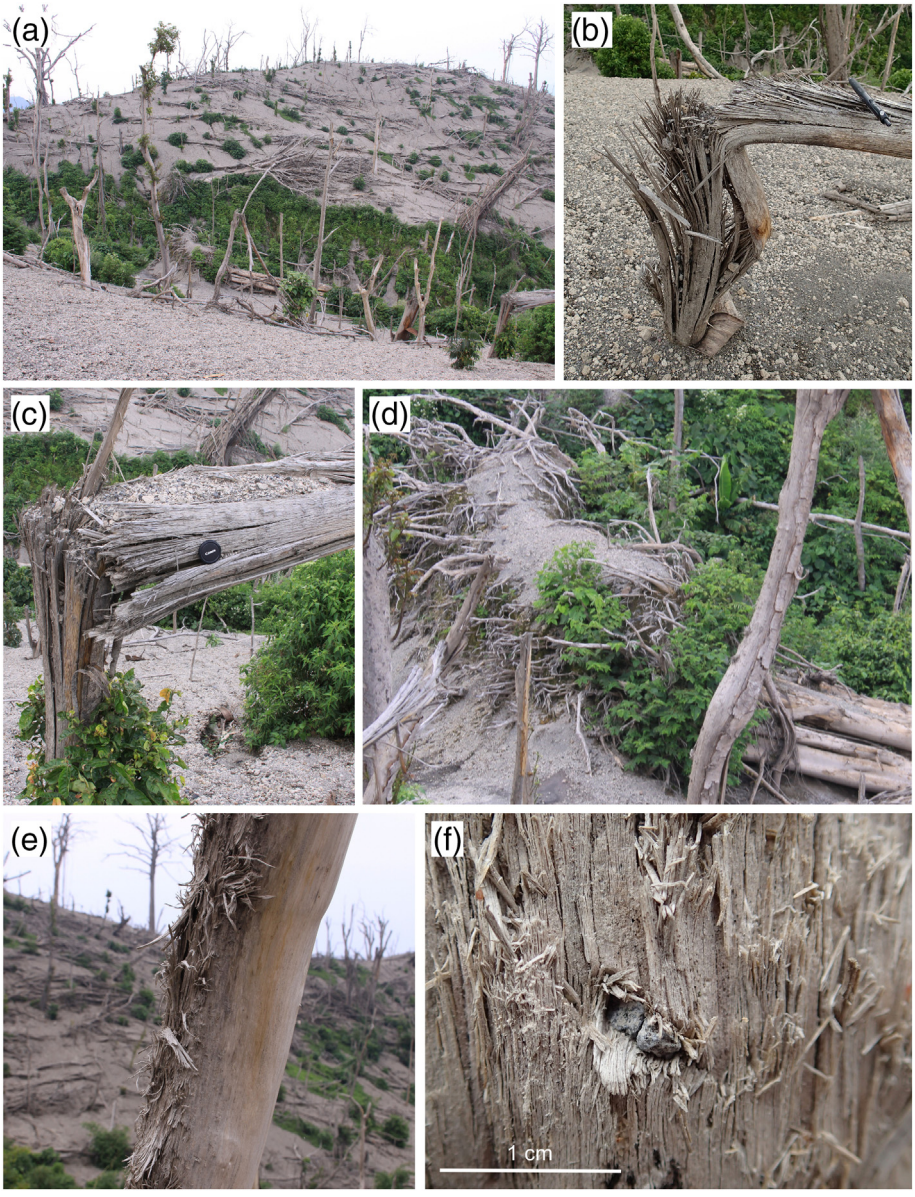

Fig. 8. Surface features on the NE edifice of Kelud volcano (around site #334). (a) Almost all the trees have fallen down, been blown away, cut, bent, or uprooted. (b) A bent tree, indicating a flow direction from the left side. (c) A bent tree with cracks filled with pumice fallout. (d) An uprooted tree. The roots are covered by pumice fallout, indicating that the uprooting occurred before the fallout. (e) Tree trunk ~10 cm in diameter, severely damaged by fragmented ejecta, as shown in panel (f). The damaged side of the tree is facing the summit crater. All photos were taken on November 22, 2014.

of Unit A plots in the same region as the basal unit of the blast deposits from the 1980 Mount St. Helens (MSH) eruption (Hoblitt et al., 1981), or the lower unit of the deposits from high-energy PDCs associated with dome destruction in the 2010 Merapi eruption (Komorowski et al., 2013) (Fig. 10). The facies, components, and grain-size characteristics of Unit A are similar to those observed in the deposits: Layer A0 of the MSH blasts (Fisher et al., 1987), Layer A of the Bezymianny blasts (Belousov, 1996), and L1–L2 of the Merapi PDCs (Komorowski et al., 2013), although the deposits from the MSH blast lack pumice (less than a few %) and they are most likely accidental lithics that were incorporated during transport. Based on previous studies, Units A_0–A_1 are interpreted to have been formed by the shearing action of the flow head (e.g., Fisher et al., 1987). Unit A_2 may correspond to the layer representing the waning of the surge current. The Kelud deposits lack the layers from a later depositional phase (e.g., Layers A1–2, Fisher et al., 1987; Layers B–C, Belousov, 1996), probably because it was a smaller-scale blast or was under different topographic effects. Trees that were most likely blown down by a large dynamic pressure current with at least a few kPa have been observed in past events of energetic pyroclastic surges or blasts (e.g., Clarke and Voight, 2000; Jenkins et al., 2013). Thus, our data shows that high-energy PDCs were probably generated during the initial phase of the eruption, but on a scale much smaller than at Mount St. Helens in 1980 or Bezyminanny in 1956, both of which caused the devastation of an area larger than 500 km^2 (Belousov et al., 2007). Units $A_{0–2}$ contain a large proportion of non-juvenile materials (i.e., dome-derived lava, and wood and leaf fragments; Fig. 11) but also juvenile pumice (20–30 wt%), indicating that the eruption began with an outburst of magmatic material.

7.1.2. Unit B

Unit B is widely distributed around the volcano, and shows typical fallout features. This implies that Unit B originated from the main phase of the eruption generating a buoyant umbrella cloud. When the classification scheme using the fragmentation and the dispersal indices (Walker, 1973) is applied, the tephra data (thickness and grain-size variations) of Unit B plots near the boundary between 'plinian' and

Please cite this article as: Maeno, F., et al., A sequence of a plinian eruption preceded by dome destruction at Kelud volcano, Indonesia, on February 13, 2014, revealed from tep..., J. Volcanol. Geotherm. Res. (2018), http://dx.doi.org/10.1016/j.jvolgeores.2017.03.002

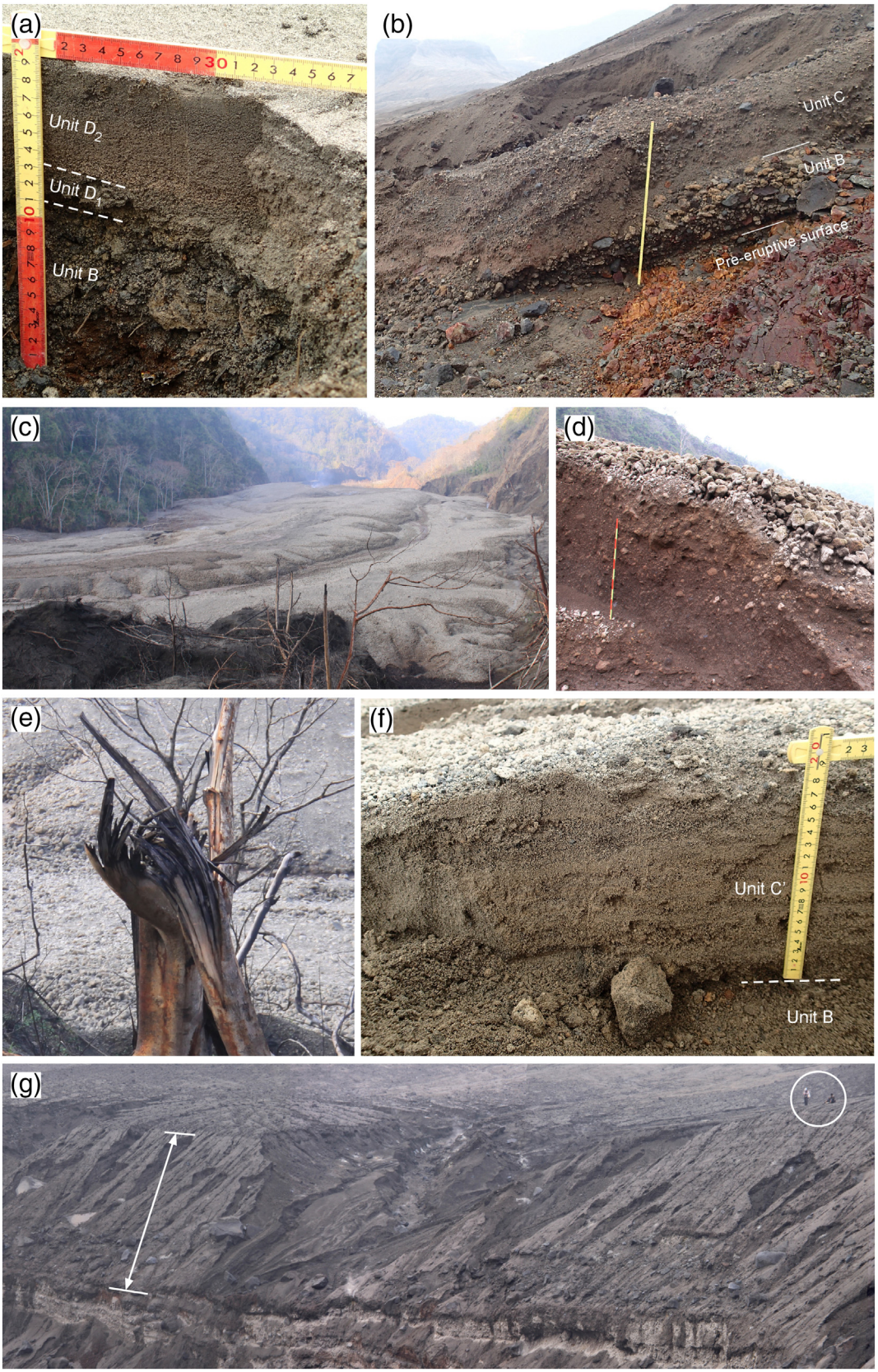

Fig. 9. Images showing products from the 2014 Kelud eruption. (a) Fallout tephra (Units B and D) at site #207 in Ngantur, taken on March 16, 2014. (b) PDC deposits (Unit C) overlying fallout deposit (Unit B) near the western rim of the summit crater at site #217, taken on March 17, 2014. (c) The western valley filled with pumiceous PDC deposits with multiple lobes at site #227, and (d) a cross-section of PDC deposits at site #224, taken on March 18, 2014. Large pumice clasts are concentrated on the surface of the deposit. (e) A partially charred fallen tree. (f) Unit C′, overlying Unit B pumice fallout, on the ridge of the western side of the summit (at location #218) taken on March 17, 2014. (g) View of the crater wall at site #215, exposing the proximal deposit produced by the 2014 eruption (indicated by white arrows), taken on March 17, 2014. The maximum deposit thickness is ~20 m. The white circle indicates a person (for scale).

Please cite this article as: Maeno, F., et al., A sequence of a plinian eruption preceded by dome destruction at Kelud volcano, Indonesia, on February 13, 2014, revealed from tep..., J. Volcanol. Geotherm. Res. (2018), http://dx.doi.org/10.1016/j.jvolgeores.2017.03.002

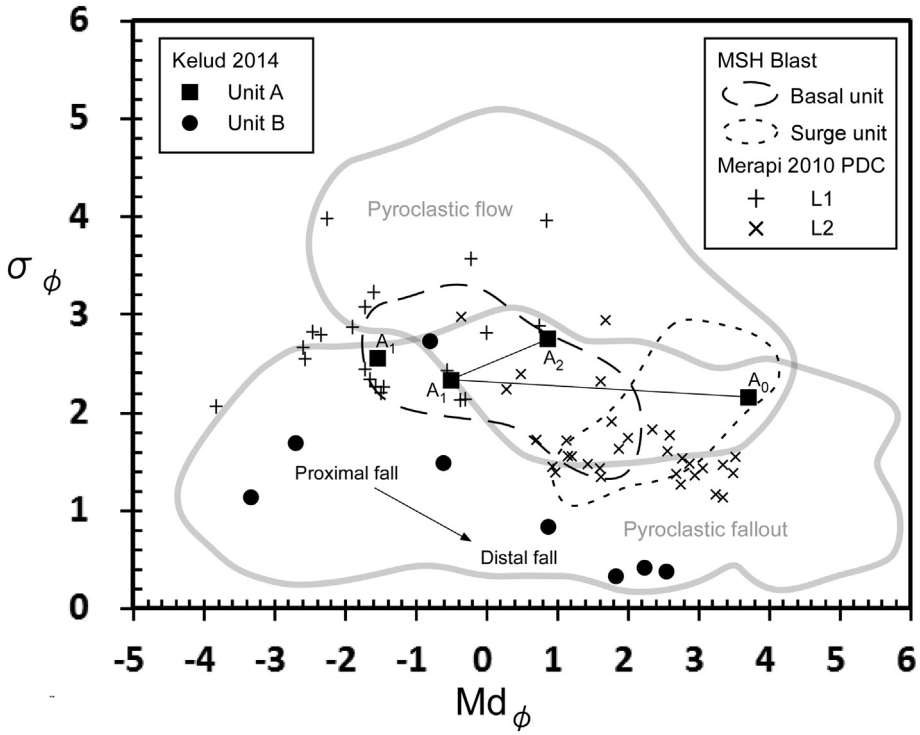

Fig. 10. Md_φ-σ_φ plot for Units A and B. Thick shaded lines indicate the areas for pyroclastic flow and fallout deposits (Walker, 1971). The blast deposits (basal and surge units) of the 1980 Mount St. Helens eruption (broken lines, Hoblitt et al., 1981) and PDC deposits (L1 and L2) of the 2010 Merapi eruption (Komorowski et al., 2013) are also shown. A solid line indicates the facies variation of Unit A_0–A_2 in the same outcrop.

'subplinian' (Fig. 13a). However, if the revised classification scheme using the clast half-distance (b_c) and the thickness half-distance (b_t) (Pyle, 1989) is applied, the tephra data plots in the 'plinian' region (Fig. 13b). Note that errors in thickness and grain-size variations (Figs. 12, 14) are considered in these plots. We refer to the main phase of the 2014 Kelud eruption as 'plinian' based on the Pyle's scheme, but we also conclude that the eruption was actually an intermediate plinian-style eruption.

The maximum clast-size of Unit B (Fig. 12) reflects the height of the eruption plume (Carey and Sparks, 1986). Although our clast data are limited, several isopleths can be determined approximately. Applying the Carey and Sparks (1986) model, the plume height (at neutral buoyancy level) is estimated as ~20 km, where 2- and 4-cm isopleths were used and the clast density of the pumice was assumed as 1500 kg/m^3. The height of the buoyant umbrella cloud was estimated as 18–19 km with possible higher ash-emission altitudes at 22–26 km based on satellite data (Kristiansen et al., 2015). The plume height estimation using clast and satellite data indicates that the major pumice fallout producing Unit B originated from the height of the eruption cloud at 18–20 km, rather than from higher altitudes of 22–26 km.

The fallout deposit extends from Kelud northeast to Surabaya and west to Yogyakarta and further westward. All the features observed in the field are consistent with the satellite data that shows that the plinian plume drifted in a strong easterly wind and dispersed mainly west of the volcano (Fig. 2). The variation shown in the grain-size histograms of Unit B may have originated during the transport and deposition of pyroclasts of various densities and shapes derived from the fragmentation of the porphyritic magma. For example, isolated pyroxene crystals are approximately three times denser than pumice. This density difference can lead to a different terminal settling velocity of the particles. The general form of the terminal settling velocity, u, of small pyroclasts can be written as $u = \sqrt{4gd(\rho_p - \rho_0)} / 3C_d\rho_0$, where g is gravitational acceleration, d is grain size, ρ_p is particle density, ρ_0 is the density of the ambient atmosphere, and C_d is the drag coefficient as a function of the particle Reynolds number (Wilson and Huang, 1979). To achieve the same settling velocity for particles with different densities, the diameter of the denser particles must be smaller to satisfy the above equation. For example, the settling velocity for −1.5φ pumice will be the same as for −0.5φ crystals. The grain-size distribution, as seen at the site 11 km west of the source (Fig. 11), indicates that the density difference produced multimodal grain-size distributions in the fallout deposits that settled from the umbrella cloud with turbulent suspension, although not all the grain-size histograms can be explained by this mechanism. In the more proximal area, within a few km from the source, the deposits are not well sorted. This was probably because some particles were deposited directly from the lower level of the eruption column, or because the particle concentration was very high. In these cases particle settling may not follow a simple settling law or assumptions (e.g., Manzella et al., 2015).

7.1.3. Units C–D

Unit C shows typical flow depositional features, as characterized by multiple pumiceous lobes. It is interpreted as valley-filled, pumice-rich PDC deposits generated by the collapse of the plinian column in the later phase of the eruption. The main dense part of the PDCs travelled in the valleys as granular flows, but may have also been accompanied by a dilute component of the current that travelled over the ridges. This is shown by blown-down trees along the valleys on the same stratigraphic level (Figs. 5, 9e) and thin stratified fine-rich deposits on the ridge (Unit C′, Fig. 9f), indicating the deposition from low-concentration pyroclastic density currents. The temperature of the pumice-rich PDCs was likely much higher than the initial PDCs, producing Unit A, because the charred materials are generally contained in Unit C. PDCs can form when the physical parameters of a plinian eruption, such as mass eruption rate, vent radius, magmatic gas content, or external water volume, fulfill certain criteria, favoring column collapse (e.g., Wilson et al., 1980; Sheridan et al., 1981; Woods, 1988). These changes may occur during the most intense, or declining, phase of a plinian eruption, as studied at Vesuvius (Carey and Sigurdsson, 1987), Katmai in 1912 (Fierstein and Hildreth, 1992), Mount Pinatubo in 1991 (Scott et al., 1996), and

Please cite this article as: Maeno, F., et al., A sequence of a plinian eruption preceded by dome destruction at Kelud volcano, Indonesia, on February 13, 2014, revealed from tep..., J. Volcanol. Geotherm. Res. (2018), http://dx.doi.org/10.1016/j.jvolgeores.2017.03.002

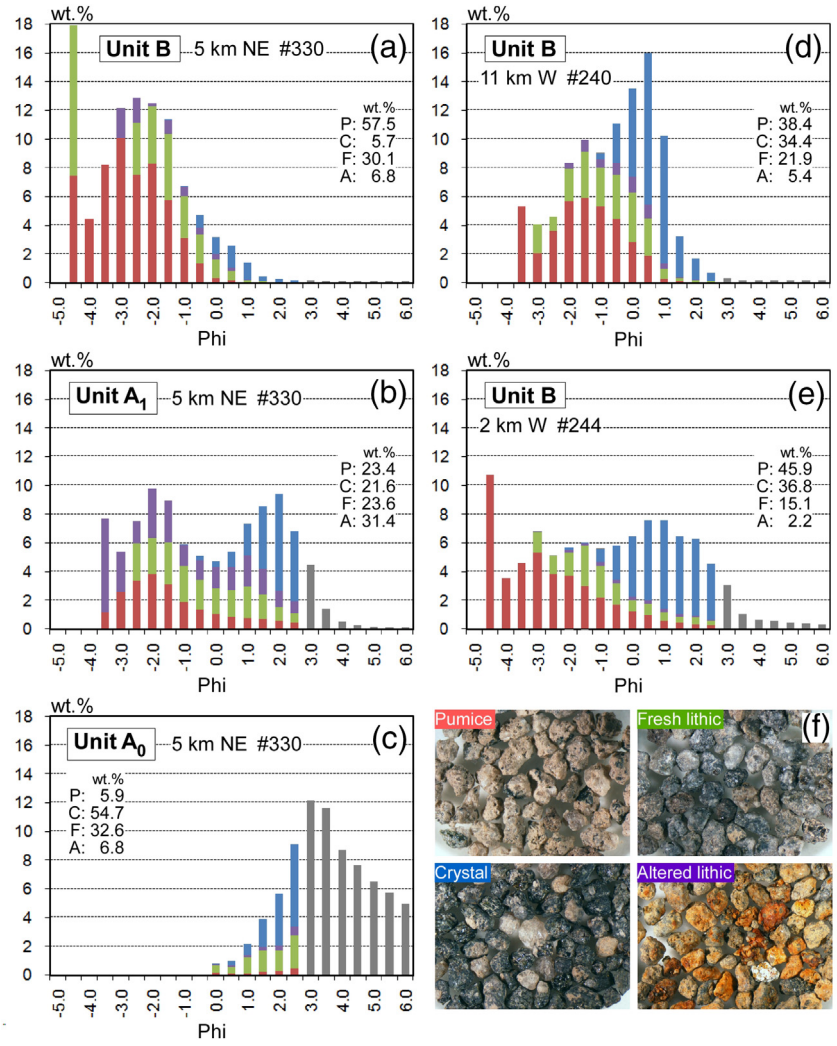

Fig. 11. Grain-size distribution and component variations for representative samples. (a) Unit B, (b) Unit A_1, and (c) Unit A_0 at site #330, 5 km NE of the source. (d) Unit B at site #240, 11 km W and (e) Unit B at site #244, 2 km W of the source. (f) Component types (0 φ, ~500 μm-sized grains): pumice (P, indicated by pink in the histograms), isolated crystals (C, blue), fresh lithic from the 2007–2008 lava (F, green), and altered lithic clasts (A, purple).

Chaiten in 2008 (Major et al., 2013). We suggest that external water was not important in the case of Kelud in 2014 because no lake-water occupied the vent before eruption. There is no clear evidence of 'wet' volcanism in the deposits, represented by specific textural and morphological features of ash particles from magma-water interaction (Houghton et al., 2015). Moreover, there are no supporting data of increases in lithic content (accessory/accidentals) related to vent enlargement in later phases of the plinian eruption. The possible causes of the column collapse during the Kelud eruption are: (1) a decrease in the mass eruption rate (and therefore a decrease of exit velocity), which reduces the entrainment of air into the plume; and (2) a decrease in the magmatic gas content at the vent, which increases the initial density of the mixture (e.g., Woods, 1988). Hargie et al. (this issue) showed a decrease in the mass eruption rate that was derived from the umbrella expansion rates sometime after ~18:00 UTC. However, it is difficult to know if this is an effect due to decreased flux at the source, or decreased flux into the umbrella cloud because of PDCs. For option (2), future geochemical analysis for time-series samples may give an insight into the cause of column collapse.

Finally, Unit D consists of ashfall deposits that most likely formed during the declining phase of the eruption, or were derived from the co-PDC liftoff plume during the deposition of Unit C. The distribution of Unit D suggests that the fine tephra in the lower-level plume at a height of a few km was affected by the southwesterly wind and transported NE as discussed in Section 7.3.

7.2. Eruption parameters

The main products from the Kelud eruption are fallout tephra and two types of PDC deposits (Units A and C). We first estimate the volume of the fallout tephra using an isopach map. The map is based primarily on the data obtained by our geological survey in early March 2014. Eyewitness reports (for distal tephra) were also used, but care was taken with such data, as identified by Nakada et al. (2016). The proximal area was mapped by 4-cm and 15-cm isopach contours (Fig. 14). The tephra data observed at Yogyakarta constrained the 1-cm isopach; however, the area covered by this isopach is minimal because the distal limit is unclear. For the more distal area, we assumed two cases with 1-mm contours (lines a and b in the isopach map in Fig. 14) based on satellite images capturing the eruption cloud spreading to the Indian Ocean (Japan Meteorological Agency, JMA, data and Kristiansen et al., 2015). However, this isopach includes a large error due to uncertainty in the distal limit over the ocean. Using the relationship between the area covered by tephra and the thickness of the deposit, we can estimate the volume of the fallout tephra deposit (Fig. 14). Here we applied three different fitting methods: exponential (Fierstein and Nathenson,

ARTICLE IN PRESS

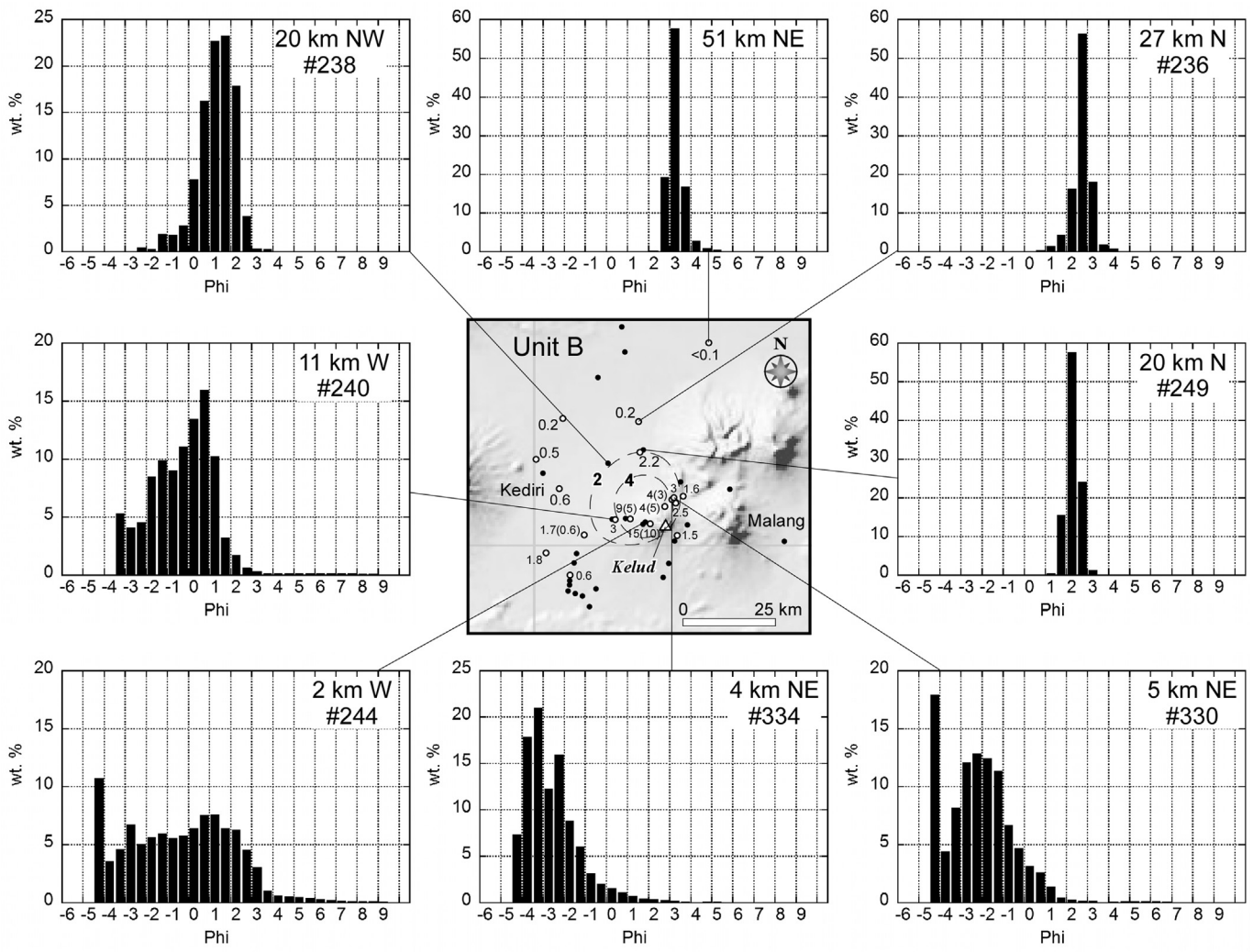

Fig. 12. Grain-size histograms for Unit B at representative sites around Kelud volcano. The maximum clast size for pumice in Unit B is also shown with 2-cm- and 4-cm-isopleths in the central map (open circles). Numbers in parentheses show lithic clast data. Units: cm.

1992), power-law (Bonadonna and Houghton, 2005), and Weibull fitting (Bonadonna and Costa, 2012). For the exponential fitting, the maximum thickness at the proximal boundary was assumed to be 3–6 m (blue squares in Fig. 14) based on the deposit of the summit crater, but we did not use the proximal assumption for the power-law and Weibull fittings. For the power-law fitting, we used 300 km and 600 km for the distal limit (black squares, corresponding to lines a and b in the isopach map of Fig. 14, respectively) based on satellite data. These three methods produced 0.27–0.47 km^3, 0.24–0.47 km^3, and 0.25–0.47 km^3, respectively. The total deposit volume of the fallout tephra was thus estimated to be 0.24–0.47 km^3. The deposit density of the fallout tephra was ~1400 kg/m^3, derived by measuring the thickness, area, and weight of the deposit at selected locations in the field. Therefore, the dense rock equivalent (DRE) volume was 0.13–0.26 km^3, assuming a magma density of 2500 kg/m^3.

To estimate the volume of the PDCs, we multiplied the area and average thickness based on field observations and a comparison between pre- and post-eruption surface images captured by satellites. The PDCs in the initial phase (Unit A) covered an area of ~6–12 km^2. Assuming an average thickness of 0.1–0.4 m, the volume was estimated to be 0.0006–0.005 km^3. The later pumice-rich, valley-filled PDC deposits covered an area of ~3 km^2. Assuming an average thickness of 2–5 m, the volume was estimated as 0.007–0.02 km^3. The volume of the PDCs that filled the summit crater was estimated as 0.006–0.008 km^3, assuming a thickness of 10–15 m. Thus, the pyroclastic density current deposit for stages 1 and 3 was estimated to be ~0.01–0.03 km^3.

The total volume including both fallout and PDCs was 0.25–0.50 km^3, corresponding to 0.14–0.28 km^3 in DRE. Therefore, we conclude that the 2014 eruption at Kelud had a VEI of 4 (eruption magnitude, M = 4.5–4.8). Based on satellite image data (Fig. 1) and remote seismic records (Caudron et al., 2015; Nakashima et al., 2016), the development of the plinian column is estimated to have lasted 2–2.5 h. Using the volume of fallout tephra and the eruption duration, the average mass eruption rate during the plinian phase was calculated as $6.5 \pm 2.8 \times 10^7$ kg/s.

7.3. Chronology based on geological and geophysical observations

The 2014 eruption at Kelud volcano can be divided into three major stages 1, 2, and 3, based on the stratigraphy of the deposit and geophysical observations (Fig. 15). Stage 1 began when high-energy PDCs formed Units A_0–A_2 and blew the trees down. The real-time camera situated at the crater captured ballistic ejecta as its final image at ~15:45 UTC, and seismometers near the summit were destroyed at 15:46 UTC, indicating that the first explosion began around this time. Our field observations suggest that the initial PDCs, containing lava fragments from the 2007–2008 dome and vesicular pumice, traveled NE by at least 6.8 km, blew down vegetation, and formed Unit A. Initially,

Please cite this article as: Maeno, F., et al., A sequence of a plinian eruption preceded by dome destruction at Kelud volcano, Indonesia, on February 13, 2014, revealed from tep..., J. Volcanol. Geotherm. Res. (2018), http://dx.doi.org/10.1016/j.jvolgeores.2017.03.002

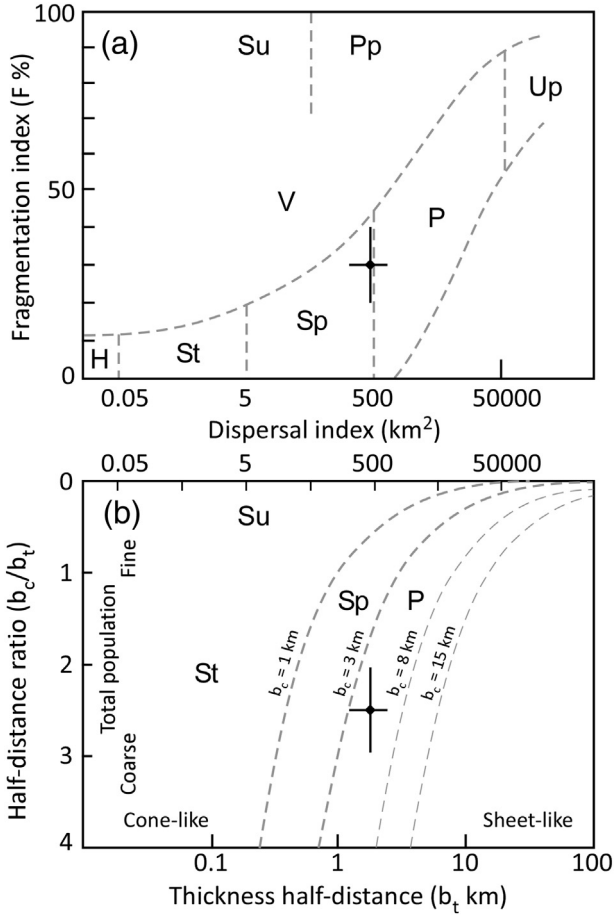

Fig. 13. Classification of the eruption style of the 2014 Kelud eruption. (a) Walker's (1973) classification using the fragmentation and dispersal indices. (b) Pyle's (1989) classification using clast half-distance (b_c) and thickness half-distance (b_t). P: Plinian; Sp: Subplinian; Pp: Phreatoplinian; Up: Ultraplinian; St: Strombolian; H: Hawaiian; V: Vulcanian; Su: Surtseyan. Diamonds with error bars indicate the data from the 2014 Kelud eruption.

the eruption could not produce a buoyant steady column from the open conduit, but generated high-energy PDCs as a result of the sudden decompression of the pressurized magma. This first explosion event may correspond to the small low-altitude plume that was detected at ~15:46 UTC by the MTSAT-2 satellite (Hargie et al., this issue), and to a brief infrasound signal followed by a weak seismic event (Caudron et al., 2015; Nakashima et al., 2016). Caudron et al. (2015) pointed out that their I_L (~15:43 UTC) and S_P1 (~15:52 UTC) signals, corresponding to a brief low-amplitude impulsive wave, are consistent with a relatively small-scale eruption. Nakashima et al. (2016) reported Total Electron Content (TEC) variations and remote seismic signals from Kelud volcano, observed by regional GNSS and broadband seismometer networks. They concluded that the first seismic signal – ground motion caused by an acoustic wave – was excited at ~15:46 UTC at the volcano, and propagated outward in the lower atmosphere at ~0.3 km/s. Based on the seismic records, they estimated that the initial explosion occurred at 15:46, followed by the start of the plinian eruption ~15 min later. Hargie et al. (this issue) analyzed volcanic lightning during the eruption that was detected by the World Wide Lightning Location Network (WWLLN), and showed that there were a few lightning strokes between 15:48–15:56 UTC, probably associated with the initial PDC phase. All these geophysical observations are consistent with our field observations and reports by observers in the Kelud Volcano Observatory.

The eruption then moved to the main plinian phase, stage 2. In this stage, the major fallout deposit (Unit B) was produced from the umbrella cloud over a wide area. The lava dome was completely destroyed by continuously ascending magma. Based on remote seismic records, Nakashima et al. (2016) estimated that the plinian eruption began at ~16:01 UTC, when the continuous tremor began. At 16:09 UTC, the first signal indicating a significant plume was observed by the MTSAT-1R satellite (Hargie et al., this issue). The plinian column rose into the stratosphere and the umbrella cloud began to spread. The eruption cloud spread radially at altitudes around 17–18 km, with the top of the umbrella cloud at 18–19 km (Kristiansen et al., 2015), and the diameter exceeding 200 km by 17:32 UTC (Fig. 1). The plume height estimation using clast data indicates that the major pumice fallout originated from the height of the eruption cloud at ~20 km. Kristiansen et al. (2015) also suggested that there were higher ash-emission altitudes between 22 and 26 km. The higher ash-emissions may correspond to the overshooting plume top, but it remains uncertain whether this was a realistic feature. Hargie et al. (this issue) showed that the lightning rate increased markedly from 16:20–17:00 and continued at a lower level until ~19:30 UTC. Seismic signals indicate that the plinian eruption lasted at least ~2 h (Caudron et al., 2015; Nakashima et al., 2016). Then, the eruption column became unstable and later collapsed.

In stage 3, the pumice-rich PDCs were formed as the column collapsed. This may have occurred around 18:00–18:30 UTC, because the continuous tremor ended at this time, suggesting the end of the vigorous plinian phase, and there are no pumice-rich PDC deposits beneath the plinian fall deposits. They travelled along the valleys from the summit area and covered them with multiple pumiceous flow lobes, forming in Unit C. Co-PDC ashfall, and/or ashfall from the low-level, vent-derived plume was transported by a southwesterly wind and formed fine ashfall layers (Unit D), mainly NE of the volcano. Although we infer that the most vigorous portion of the plinian eruption ended at 18:00–18:30 UTC, the plume continued to expand and drifted west (Fig. 1), and distal ashfall continued for several hours over a wide area of Java.

The tephra dispersal process and deposit formation was significantly affected by the local winds around Kelud volcano. The wind velocity fields at the 100-hPa and 700-hPa levels at 18:00 UTC on February 13, 2014 (1:00 local time) over Kelud volcano were obtained from the real-time Grid Point Values (GPV) data provided by the global spectral model (with 1.25° longitude-latitude grids) of JMA (Tanaka et al., 2016). This data are comparable to the radiosonde data from Surabaya Juanda airport at 12:00 UTC on February 13 and 0:00 UTC on February 14 (obtained from NOAA's Earth System Research Laboratory). According to the GPV/JMA data, at the time of the eruption the 100 hPa wind vector field (at an altitude of ~16.5 km) indicated strong easterly winds blowing at 25 m/s over Java (Tanaka et al., 2016). In contrast, the 700 hPa wind vector field (at an altitude of ~3 km) showed a southwesterly flow of 9 m/s over Kelud volcano. The wind field above Kelud volcano is shown in Fig. 16. The umbrella cloud at the higher altitude (~17 km a.s.l.) during the main plinian stage was affected by strong easterly winds as observed by satellite images. However, fine ash in the lower-altitude plume(s) was affected by the southwesterly wind and preferentially transported NE. Based on field stratigraphic relationships, the distribution of the upper fine ash layers (Unit D, Figs. 7, 8) was caused by ashfall from low-level plumes, originating from the waning stage of the plinian column, or liftoff from PDCs.

7.4. Initial dome destruction and directed pyroclastic density currents

The opening phase of the 2014 Kelud eruption was characterized by high-energy PDCs associated with the destruction of the pre-existing lava dome. Vent-derived surges were reported during the opening phase of the 1990 Kelud eruption. At that time, the volcano contained a crater lake, and water likely had free access to the vent; hence the initial explosions can be considered phreatomagmatic (Bourdier et al., 1997). The 2014 eruption began without a crater lake, and therefore a phreatomagmatic origin is unlikely. In some cases, PDCs can precede the main phase of the explosive event. They are represented by high-energy PDCs (called blasts) as observed at Mount Lamington in 1951

Please cite this article as: Maeno, F., et al., A sequence of a plinian eruption preceded by dome destruction at Kelud volcano, Indonesia, on February 13, 2014, revealed from tep..., J. Volcanol. Geotherm. Res. (2018), http://dx.doi.org/10.1016/j.jvolgeores.2017.03.002

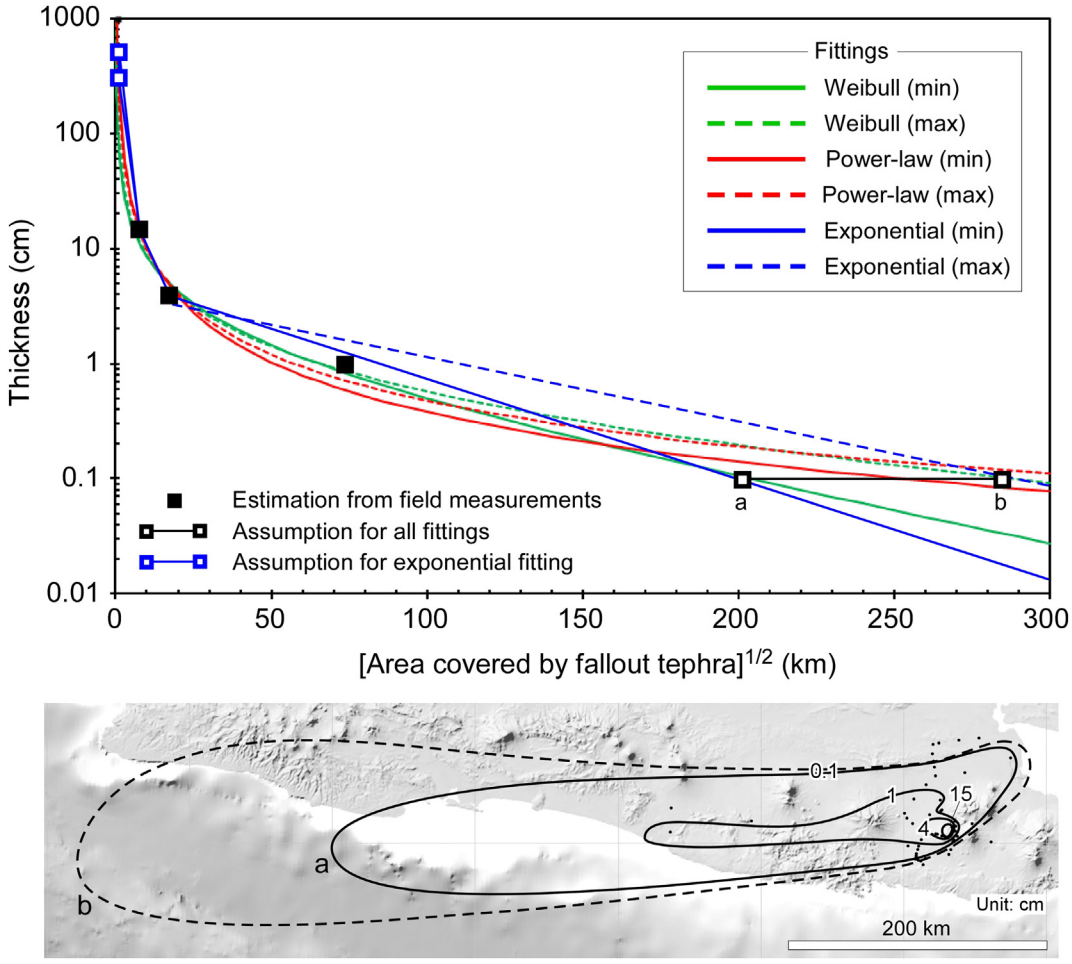

Fig. 14. Tephra thinning trend for the 2014 Kelud eruption (top) and isopach map (bottom) used for volume estimates. Deposit thicknesses at individual locations are shown in Fig. 2. Three fitting methods were applied: Weibull, power-law, and exponential fittings. For the exponential fitting, the maximum thickness at the proximal boundary was assumed to be 3–6 m (blue squares), but the proximal assumption was not used for the power-law and Weibull fittings. For all fittings, minimum calculations were made using the 0.1 cm contour indicated by a solid line (a) in the lower panel. Maximum calculations were made using the 0.1 cm contour indicated by a broken line (b). See text for details.

(Taylor, 1958), Bezymianny volcano in 1956 (Belousov, 1996), Arenal volcano in 1968 (Alvarado et al., 2006), Mount St. Helens in 1980 (Kieffer, 1981; Hoblitt and Miller, 1984), and Mount Pinatubo (Hoblitt et al., 1996), all of which are associated with the growth of a lava dome or cryptodome just prior to the onset of the plinian phase. Sudden decompression of the pressurized dome lava due to residual gas in the highly viscous magma is thought to be a triggering mechanism of high-energy PDCs (e.g., Fink and Kieffer, 1993). They may be highly directional when triggered by the collapse of the flank of a stratovolcano such as Mount St Helens and Bezymianny, or not associated with slope failure but caused by the collapse of the lava dome as in the Lamington, Arenal, and Pinatubo cases. Gravitational collapse of a growing dome on a slope can also trigger sudden decompression and high-energy PDCs (e.g., Boudon and Lajoie, 1989). The pre-existing lava dome is thus a key to understanding the mechanism of explosive plinian eruptions, although the duration between dome growth and the plinian phase can vary from days to years (Newhall and Melson, 1983; Ogburn et al., 2015).

The sequence of the 2014 Kelud eruption is similar to that seen in past plinian events associated with dome growth. However, there is a difference in terms of duration between the dome growth and the plinian phase. At Kelud volcano, the lava dome was formed in 2007–2008 (Jeffery et al., 2013) followed by a 6-year dormant period before the 2014 event. Therefore, most of the dome was likely already degassed. Moreover, gravitational collapse is unlikely to occur on the crater floor. However, the deep interior of the dome-conduit system may still be hot. We propose that the initial phase of the 2014 Kelud eruption is similar to the vent-opening phase of the Chaiten eruption in 2008. At Chaiten, directional dilute PDCs covering an area of ~4 km^2 occurred through the old lava dome (Major et al., 2013). Chaiten's PDCs were much smaller than those in the Kelud eruption. Major et al. (2013) suggested that the opening of pathways through the old lava dome produced narrow, asymmetrically-shaped vents, and that the geometries of those vents were the main factor that controlled the PDCs in the Chaiten eruption.

The PDC deposit (Unit A) from the 2014 eruption contains a significant amount of pumice (20–30 wt%), indicating that newly ascended magma triggered the destruction of the dome. Here we propose a mechanism where newly ascended magma fractured the old lava dome and produced a new pathway to the surface, resulting in rapid decompression of new magma and the subsequent eruption that destroyed the old lava dome. In this process, the lava dome may act as a solid cap on the vertical conduit and promote pressurization of the ascending magma, preventing effective degassing (e.g., Sparks, 1997; Preece et al., 2016).

Based on the above, we propose the following scenario for the 2014 Kelud eruption: the initial vent position was on the northern side of the dome and was partially destroyed during the initial phase. The confined exit condition channeled the PDCs north. Once the initial vent was established, a rapid decompression triggered fragmentation of the magma, resulting in the onset of the explosive plinian phase. During the plinian phase, the vent was enlarged and the dome was completely

Please cite this article as: Maeno, F., et al., A sequence of a plinian eruption preceded by dome destruction at Kelud volcano, Indonesia, on February 13, 2014, revealed from tep..., J. Volcanol. Geotherm. Res. (2018), http://dx.doi.org/10.1016/j.jvolgeores.2017.03.002

ARTICLE IN PRESS

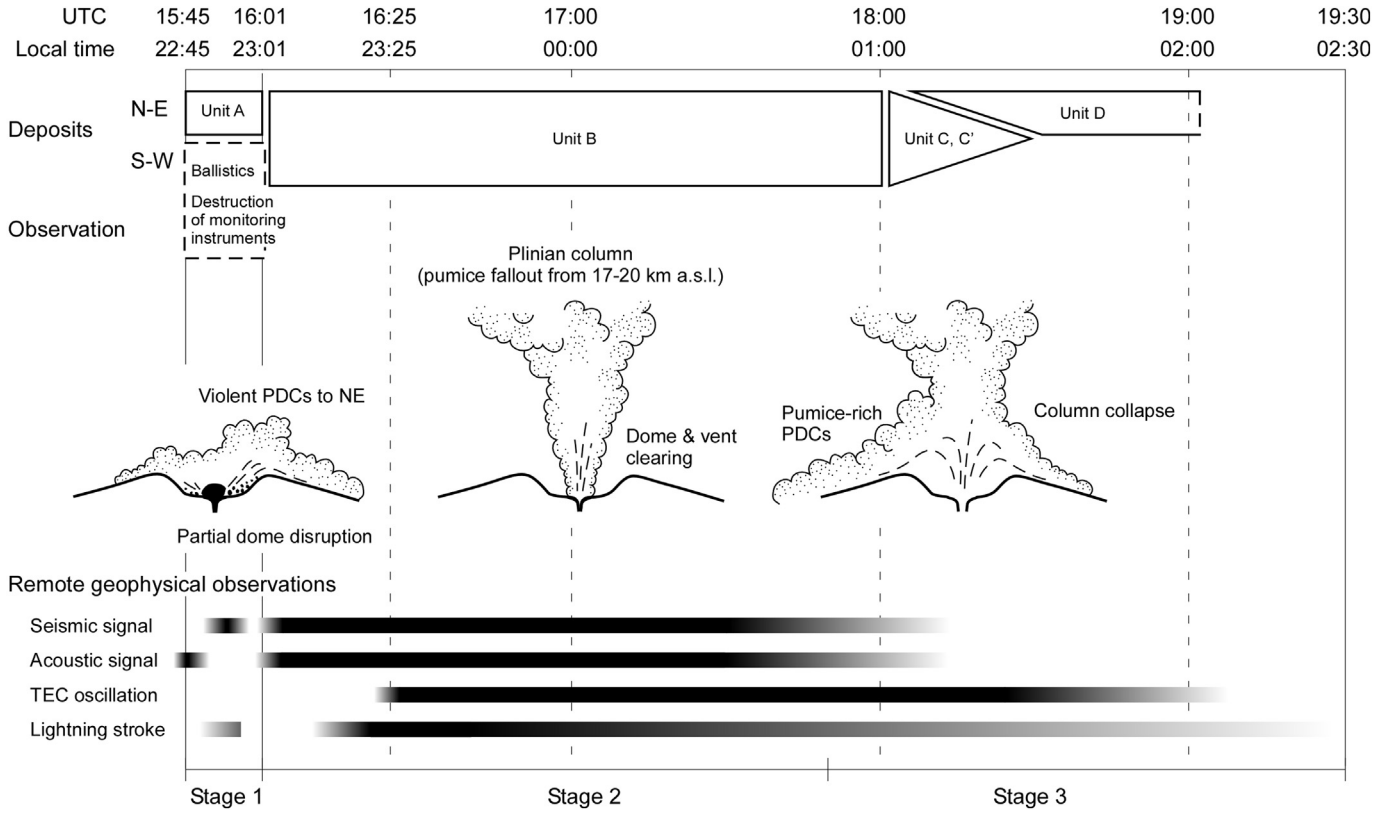

Fig. 15. Illustration of the eruption sequence of the 2014 Kelud eruption, viewed from geological and geophysical observations. Stage 1 shows a partial, directional dome destruction generating high-energy PDCs toward the NE. Stage 2 depicts the main explosive plinian column stage. Stage 3 illustrates the plinian column collapse and generation of pumiceous valley-filled PDCs. The seismic and acoustic signals (bottom) are from Caudron et al. (2015). The Total Electron Content oscillation data are from Nakashima et al. (2016). The lightning stroke data are from Hargie et al. (this issue). Plume height is based on Kristiansen et al. (2015).

destroyed, resulting in the development of the vertical eruption column. There was a ~ 15 min pause between the initial high-energy PDC (15:46) and the start of the pumice-rich, vertical column (16:01 UTC). At MSH, there was also a pause between the blast and the vent-derived plume (minutes to 10s of minute) (Criswell, 1987).

It is also important to consider the geometry of the summit crater and valleys to understand what caused the high-energy PDCs to extend to the NE. The summit crater area of Kelud volcano is basically confined by the crater wall, which rises up to ~500 m above the crater floor. On the western and northern sides, the crater wall is partially depressed, with deep valleys developing toward the foot of the volcano (indicated by arrows in Fig. 17a). The western crater wall (~1250 m a.s.l.) is lower than the northern side (~1400 m a.s.l.). These topographic depressions and valleys may act as confined channels, guiding the PDCs along specific routes. If the entire dome is destroyed instantaneously, a blast would expand in all directions and the PDCs will tend to travel along the topographic lows. Therefore, the disturbed area covered by deposits would be more likely to extend toward the western side of the volcano rather than the other more elevated areas. However, the absence of Unit A on the western side indicates that the initial PDCs flowed mainly NE, drained from the topographic depression, and expanded along the valley heading N, although the northern crater rim is higher than the western rim. Therefore, we infer that the initial dome destruction started from the northern side and a PDC was generated mainly toward the north.

Analysis of the samples from Unit A and the estimate of erupted volume also indicate the partial destruction of the lava dome. The component analysis of the initial PDCs in the NE area shows that the dome-derived lithic (non-juvenile) material comprised approximately 70–80 wt% of the deposit. If we assume this proportion of dome material is representative, the volume of the collapsed dome is estimated to be 0.0003–0.003 km^3. This corresponds to 1–9 vol% of the pre-existing lava dome (~0.035 km^3, Siebert et al., 2011). This estimate suggests that the lava dome was only partially destroyed in the initial PDC phase. However, plinian fallout deposits (0.13–0.26 km^3 in DRE) contain 15–30 wt% dome-derived lithic material, corresponding to 0.02–0.08 km^3. Therefore, the rest of the dome and the pre-existing solidified magma occupying the shallow conduit may have been blown out completely during the plinian phase.

7.5. Implications for volcanic hazards and impacts

The 2014 Kelud eruption shows that a pre-existing lava dome can dramatically affect the dynamics and evolution of a volcanic eruption, although the time period after dome formation is also an important factor (Newhall and Melson, 1983). A rapid decompression of the dome-conduit system that is triggered by newly ascended magma can destroy the lava dome and generate high-energy PDCs. The high-energy PDCs travel at high velocities as turbulent suspensions. The velocity of such currents leaves a trail of destruction on the ground, blowing down trees and vegetation (Valentine, 1998; Clarke and Voight, 2000). PDC velocities can reach over 200 m/s in large-scale blast eruptions associated with flank collapse (e.g., Kieffer and Sturtevant, 1988). The 2014 Kelud eruption was on a much smaller scale than this type of blast, but demonstrated the severe hazards posed by high-energy PDCs around the volcano. Our observations of PDCs associated with a plinian event, as observed in the 2014 eruption, are important for evaluating potential hazards at Kelud volcano.

In the current hazard map of Kelud volcano (Mulyana et al., 2004), the area at risk from ejected rock fragments and hot mud is defined by a 2-km radius from the vent in the summit crater. The area potentially affected by heavy ash fall, hot mud, and ejected rock fragments is defined by a 5-km radius from the same point. The dark-gray area in Fig. 17b (the summit crater and western valley) shows the area at risk of

Please cite this article as: Maeno, F., et al., A sequence of a plinian eruption preceded by dome destruction at Kelud volcano, Indonesia, on February 13, 2014, revealed from tep..., J. Volcanol. Geotherm. Res. (2018), http://dx.doi.org/10.1016/j.jvolgeores.2017.03.002

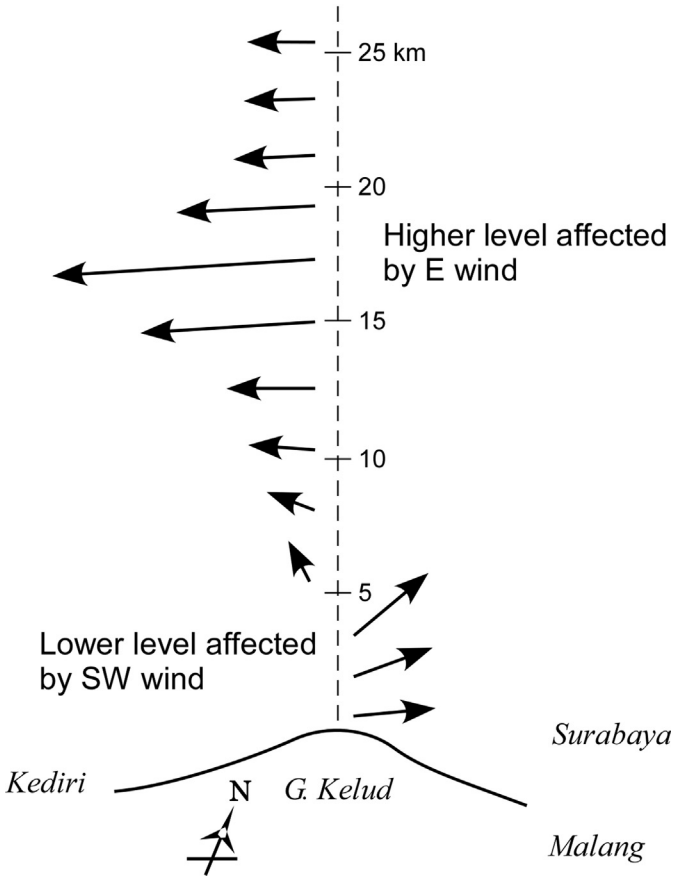

Fig. 16. Estimated wind pattern above Kelud volcano at the time of the 2014 eruption. The higher level (~17 km) is affected by winds from the east, and the lower level (~3 km) is affected by winds from SW. This wind field is based on the GPV/JMA data (Tanaka et al., 2016) and the radiosonde data from Surabaya Juanda airport at 12:00 UTC on February 13 and 00:00 UTC on February 14 (obtained from NOAA's Earth System Research Laboratory).

pyroclastic flows, toxic gas, eruption lahars, and potential lava flows. The light-gray area (in all directions) shows the area that is potentially affected by pyroclastic and lava flows, and eruption and rain lahars. During the 2014 eruption, PDCs caused a threat NE of the crater, extending along the ridges over 6 km from the summit crater. The village of Ngantur is located only 2 km from the outer extent of these PDCs. If the PDC had extended slightly beyond this boundary, the village could have been severely damaged. In previous Kelud eruptions, this type of high-energy PDC associated with dome destruction was not reported. This potential effect of PDCs, as well as the effect of topography, particularly the valleys that channel the PDCs outside the summit area, should be considered when deciding the hazard zonation around Kelud volcano.

The 20th-century eruptions at Kelud volcano were characterized by VEI 4-scale plinian eruptions accompanied by PDCs (1901, 1919, 1951, 1966, and 1990), or smaller-scale dome-building (1920, and 2007–2008). The 2014 eruption with a total volume of 0.14–0.28 km^3 (in DRE) was the largest since 1919 and provided an important opportunity to examine the sequence of a plinian eruption and its associated hazards in detail. The recurrence history of a plinian eruption and dome formation at Kelud volcano indicates that an eruption of similar type and scale to the 2014 event could occur again in the future. The eruption volume that defines the scale of eruption is important for determining the impact of the eruption over a wide area. The widespread tephra distribution seen in past eruptions, particularly in 1919 and 1951, is similar to that of the 2014 eruption (Kemmerling, 1921; Alzwar, 1985; Wirakusumah, 1991). Thus, it seems that fallout tephra from Kelud volcano is often significantly affected by prevailing easterly winds, and dispersed over a wide area of Java. In addition to the effect of the eruption volume and wind conditions on tephra dispersal, the crater condition at the summit is another key factor that determines the course of the eruption. The presence or absence of a lava dome or crater lake at the summit area will affect the eruption dynamics. A lava dome can change the pressurization process of ascending magma and can trigger high-energy PDCs, as in the 2014 eruption. A crater lake can cause initial explosive magma-water interaction and also trigger lahars, as in the past eruptions at Kelud volcano. The findings from the 2014 event have important implications that can be used to construct more sophisticated event trees and assess future volcanic hazards of Kelud volcano, and other active volcanoes that have the potential to generate both explosive and effusive eruptions.

8. Conclusions

We have documented the sequence of the 2014 plinian event at Kelud volcano based on a geological study of the eruptive products, analysis of satellite images of the eruption plume, and surface features of the volcanic edifice before and after the eruption. Based on this study, the 2014 deposits can be divided into four major depositional units (Units A, B, C, and D). The plinian eruption was preceded by the partial destruction of the lava dome produced in 2007–2008, which led to the generation of directional, high-energy PDCs with a maximum runout distance of ~6.8 km toward the NE. The PDCs produced a series of deposits (Units A_0–A_2) and caused surface damage (blown-down trees and vegetation) over an area of 12 km^2 (stage 1). The main phase of the eruption was characterized by a strong eruption plume that produced widespread fallout tephra (Unit B) over East and Central Java (stage 2). The tephra dispersal was greatly affected by the wind pattern above the volcano. In the later phase of the eruption, dense PDCs were generated by column collapse (stage 3), filling the nearby valleys with pumiceous lobate deposits (Unit C). The declining phase produced fine ashfall (Unit D_{1-2}) from a low-level plume and/or co-PDC ash. This eruption process is also supported by geophysical data, including remote seismic and infrasound signals, TEC variation, lightning strokes, and satellite observations. The initial high-energy PDCs and fallout tephra contained juvenile pumice and dome-derived lithic clasts, and isolated crystals originated from the fragmentation of porphyritic magma. The eruptive products suggest that newly ascended magma triggered the partial destruction of the lava dome accompanied by the high-energy PDCs, and the dome was completely destroyed during the climactic plinian phase. Thus, the pre-existing lava dome significantly affected the course of the eruption. This type of eruption sequence has not been previously documented in the historical records of Kelud volcano activity.

The total volume of erupted material was estimated as 0.25–0.50 km^3 (bulk deposit volume), corresponding to 0.14–0.28 km^3 in DRE, and the mean eruption rate as $6.5 \pm 2.8 \times 10^7$ kg/s. The scale of the 2014 eruption had a VEI of 4, and was one of the largest eruptions at Kelud volcano over the past century. The eruption sequence and estimated physical parameters of the 2014 eruption can be used as a guide for assessing future volcanic activity and potential hazards at Kelud volcano.

Supplementary data to this article can be found online at http://dx.doi.org/10.1016/j.jvolgeores.2017.03.002.

Acknowledgements

We are very grateful to the Centre for Volcanology and Geological Hazard Mitigation (CVGHM), Indonesia, for their assistance with our field surveys around Kelud volcano. Special thanks to A. Harijoko of Gadjah Mada University and R. Purta of the CVGHM for providing tephra information soon after the 2014 Kelud eruption. We also thank A.R. Van Eaton and R. Gertisser for their constructive reviews that improved the quality of the paper. This work was supported by the SATREPS project 'Integrated Study on Mitigation of Multimodal Disasters Caused by

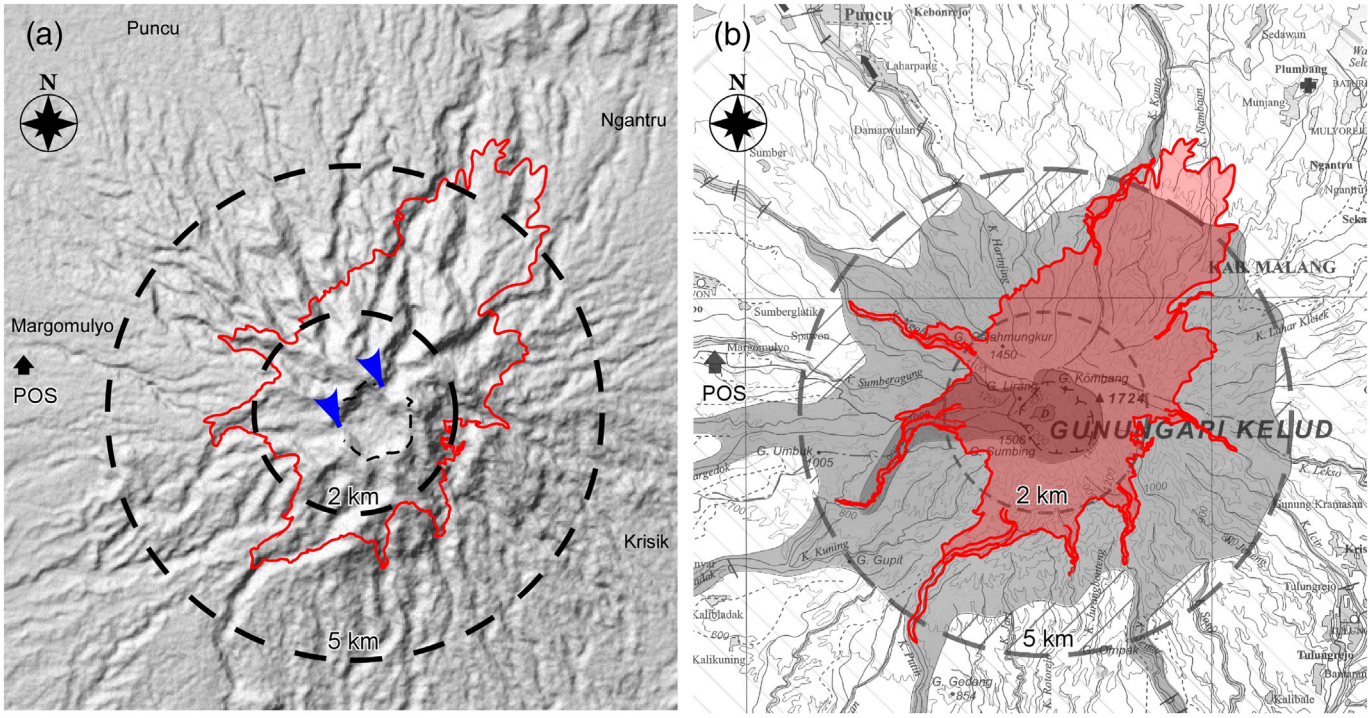

Fig. 17. Distribution of PDCs from the 2014 Kelud eruption and its comparison with topographic and hazard maps. (a) Shaded-relief topographic map of Kelud volcano. The map was made using the GDEM that is a product of the Ministry of Economy, Trade and Industry, Japan and the NASA Jet Propulsion Laboratory. Blue arrows indicate topographic lows connected to the western and northern valleys outside the summit crater. The solid red line indicates the distribution of blown-down trees. (b) Hazard map of Kelud volcano showing the distribution of PDCs from the 2014 eruption. Dashed lines indicate the potential damaged areas with a radius of 5 km and 2 km. Red shaded area indicates the distribution of PDCs from the 2014 eruption. (For interpretation of the references to color in this figure, the reader is referred to the web version of this article.)

Ejection of Volcanic Products' funded by the Japan International Cooperation Agency (JICA) and the Japan Science and Technology Agency (JST), and was also partially supported by Grant-in-Aid for scientific research (No. 15K01246) from the Ministry of Education, Culture, Sports, Science, and Technology, Japan.

References

Alvarado, G.E., Soto, G.J., Schimincke, H.-U., Bolge, L.L., Sumita, M., 2006. The 1968 andesitic lateral blast eruption at Arenal volcano, Costa Rica. J. Volcanol. Geotherm. Res. 157, 9–33.

Alzwar, M., 1985. Gunung Kelud. Berita Berkala Vulkanologi, Edisi Khusus, 108, Direktorat Vulkanologi, Volcanol. Surv. Indonesia, Bandung. p. 60.

Belousov, A., 1996. Deposits of the 30 March 1956 directed blast at Bezymianny volcano, Kamchatka, Russia. Bull. Volcanol. 57, 649–662.

Belousov, A., Voigt, B., Belousova, M., 2007. Directed blasts and blast-generated pyroclastic density currents: a comparison of the Bazymianny 1956, Mount St Helens 1980, and Soufriere Hills, Montserrat 1997 eruptions and deposits. Bull. Volcanol. 69, 701–740.

Bonadonna, C., Costa, A., 2012. Estimating the volume of tephra deposits: a new simple strategy. Geology 40, 415–418.

Bonadonna, C., Houghton, B.F., 2005. Total grain-size distribution and volume of tephrafall deposit. Bull. Volcanol. 67, 441–456.

Boudon, G., Lajoie, J., 1989. The 1902 Peleean deposits in the Fort Cemetery of St. Pierre, Martinique: a model for the accumulation of turbulent nuees ardentes. J. Volcanol. Geotherm. Res. 38, 113–129.

Bourdier, J.-L., Pratomo, I., Thouret, J.-C., Boudon, G., Vincent, P.M., 1997. Observations, stratigraphy and eruptive processes of the 1990 eruption of Kelut volcano, Indonesia. J. Volcanol. Geotherm. Res. 79, 181–203.

Carey, S., Sigurdsson, H., 1987. Temporal variations in column height and magma discharge rate during the 79 A.D. eruption of Vesuvius. Geol. Soc. Am. Bull. 99, 303–314.

Carey, S., Sigurdsson, H., 1989. The intensity of plinian eruption. Bull. Volcanol. 51, 28–40.

Carey, S., Sparks, R.S.J., 1986. Quantitative models of the fallout and dispersal of tephra from volcanic eruption columns. Bull. Volcanol. 48, 109–125.

Caudron, C., Taisne, B., Garces, M., Alexis, L.P., Mialle, P., 2015. On the use of remote infrasound and seismic stations to constrain the eruptive sequence and intensity for the 2014 Kelud eruption. Geophys. Res. Lett. 42, 6614–6621.

Cioni, R., Marianelli, P., Sbrana, A., 1992. Dynamics of the A.D. 79 eruption: stratigraphyic, sedimentological and geochemical data on the succession from the Somma-Vesuvius southern and eastern sectors. Acta Volcanol. 2, 109–123.

Cioni, R., Pistolesi, M., Rosi, M., 2015. Plinian and subplinian eruptions. In: Sigurdsson, H., Houghton, B.F., Rymer, H., Stix, J., McNutt, S.R. (Eds.), The Encyclopedia of Volcanoes, second ed. Academic Press, San Diego, California, pp. 519–535.

Clarke, A.B., Voight, B., 2000. Pyroclastic current dynamic pressure from aerodynamics of tree or pole-down. J. Volcanol. Geotherm. Res. 100, 395–412.

Criswell, C.W., 1987. Chronology and pyroclastic stratigraphy of the May 18, 1980, eruption of Mount St. Helens, Washington. J. Geophys. Res. 92 (B10), 10237–10266.

De Belizal, E., Lavigne, F., Gaillard, J.C., Grancher, D., Pratomo, I., Komorowski, J.-C., 2012. The 2007 eruption of Kelut volcano (East Java, Indonesia): phenomenology, crisis management and social response. Geomorphology 136, 165–175.

Fierstein, J., Hildreth, W., 1992. The plinian eruptions of 1912 at Novarupta, Katmai National Park, Alaska. Bull. Volcanol. 54, 646–684.

Fierstein, J., Nathenson, M., 1992. Another look at the calculation of fallout tephra volumes. Bull. Volcanol. 54, 156–167.

Fink, J.H., Kieffer, S.W., 1993. Estimatet of pyroclastic flow velocities resulting from explosive decompression of lava domes. Nature 263, 612–615.

Fisher, R., Glicken, H.X., Hoblitt, R.P., 1987. May 18, 1980, Mount St. Helens deposits in South Coldwater Creek, Washington. J. Geophys. Res. 92 (B10), 10267–10283.

Hargie, K.A., Van Eaton, A.R., Ewert, J.W., Holzworth, R.H., Mastin, L.G., Pavolonis, M., Schneider, D.J., Globally detected volcanic lightning and umbrella dynamics during the 2014 eruption of Kelud, Indonesia. J. Volcanol. Geotherm. Res. (this issue).

Hoblitt, R.P., Miller, D.C., 1984. Comments and reply on "Mount St. Helens 1980 and Mount Pelee 1902 – flow or surge?". Geology 12, 692–693.

Hoblitt, R.P., Miller, D.C., Vallance, J.E., 1981. Origin and stratigraphy of the deposits produced by the May 18 directed blast. In: Lipman, P.W., Mullineaux, D.R. (Eds.), The 1980 Eruptions of Mount St. Helens, Washington. 1250. US Geol. Surv. Prof. Rep., pp. 401–419.

Hoblitt, R.P., Wolfe, E.W., Scott, W.E., Couchman, M.R., Pallister, J.S., Javier, D., 1996. The preclimactic eruptions, June 1991, Monut Pinatubo, Philippines. In: Newhall, C.G., Punongbayan, R.S. (Eds.), Fire and Mud: Eruptions and Lahars of Mount Pinatubo, Philippines. University of Washington Press, pp. 457–511.

Houghton, B., White, J.D.L., Van Eaton, A.R., 2015. Phreatomagmatic and related eruption styles. In: Sigurdsson, H., Houghton, B.F., Rymer, H., Stix, J., McNutt, S.R. (Eds.), The Encyclopedia of Volcanoes, second ed. Academic Press, San Diego, California, pp. 537–552.

Inman, D.L., 1952. Measures of describing the size distribution of sediments. J. Sediment. Petrol. 22, 125–145.

Jeffery, A.J., Gertisser, R., Troll, V.R., Jolis, E.M., Dahren, B., Harris, C., Tindle, A.G., Preece, K., O'Driscoll, B., Humaida, H., Chadwick, J.P., 2013. The pre-erupting magma plumbing sytem of the 2007-2008 dome-forming eruption of Kelut volcano, East Java, Indonesia. Contrib. Mineral. Petrol. 16, 275–308.

Jenkins, S., Komorowski, J.-C., Baxter, P., Spence, R., Picquout, A., Lavigne, F., Surono, 2013. The Merapi 2010 eruption: an interdisciplinary impact assessment methodology for studying pyroclastic density current dynamics. J. Volcanol. Geotherm. Res. 261, 316–329.

Kemmerling, G.L.L., 1921. De uitbarsting van den G. Keloet in den nacht van den 19den op den 20sten Mei 1919. Vulkanol. Meded. No. 2.

Please cite this article as: Maeno, F., et al., A sequence of a plinian eruption preceded by dome destruction at Kelud volcano, Indonesia, on February 13, 2014, revealed from tep..., J. Volcanol. Geotherm. Res. (2018), http://dx.doi.org/10.1016/j.jvolgeores.2017.03.002

ARTICLE IN PRESS

Kieffer, S.W., 1981. Fluid dynamics of the May 18 blast at Mt St Helens. In: Lipman, P.W., Mullineaux, D.R. (Eds.), The 1980 Eruptions of Mount St. Helens, Washington. 1250. US Geol. Sur. Prof. Pap., pp. 379–400.
Kieffer, S.W., Sturtevant, B., 1988. Erosional furrows formed during the lateral blast at Mount St. Helens, May 18, 1980. J. Geophys. Res. 93 (B12), 14793–14816.
Komorowski, J.-C., Jenkins, S., Baxter, P.J., Picquout, A., Lavigne, F., Charbonnier, S., Gertisser, R., Preece, K., Cholik, N., Budi-Santoso, A., Surono, 2013. Paroxysmal dome explosion during the Merapi 2010 eruption: processes and facies relationships of associated high-energy pyroclastic density currents. J. Volcanol. Geotherm. Res. 261, 260–294.
Kristiansen, N.I., Prata, A.J., Stohl, A., Carn, S.A., 2015. Stratospheric volcanic ash emissions from the 13 February 2014 Kelut eruption. Geophys. Res. Lett. 42, 588–596.
Major, J.J., Pierson, T.C., Hoblitt, R.P., Moreno, H., 2013. Pyroclastic density currents associated with the 2008–2009 eruption of Chaiten Volcano (Chile): forest disturbances, deposits, and dynamics. Andean Geol. 40, 324–358.
Manzella, I., Bonadonna, C., Phillips, J.C., Monnard, H., 2015. The role of gravitational instabilities in deposition of volcanic ash. Geology 43, 211–214.
Mulyana, A.R., Nasution, A., Martono, A., Sumpena, A.D., Purwoto, Santoso, M.S., 2004. Volcanic Hazards Map of Kelud Volcano, East Java Province. Direktorat Vulkanologi dan Mitigasi Bencana Geologi.
Nakada, S., Zaennudin, A., Maeno, F., Yoshimoto, M., Hokanishi, N., 2016. Credibility of volcanic ash thickness reported by the media and local residents following the 2014 eruption of Kelud volcano, Indonesia. J. Disaster Res. 11, 53–59.
Nakashima, Y., Heki, K., Takeo, A., Cahyadi, M.N., Aditiya, A., Yoshizawa, K., 2016. Atmospheric resonant oscillations by the 2014 eruption of the Kelud volcano, Indonesia, observed with the ionosphereic total electron contents and seismic signals. Earth Planet. Sci. Lett. 434, 112–116.
Newhall, C.G., Melson, W.G., 1983. Explosive activity associated with the growth of volcanic domes. J. Volcanol. Geotherm. Res. 17, 111–131.
Newhall, C.G., Self, S., 1982. The volcanic explosivity index (VEI): an estimate of explosive magnitude for historical volcanism. J. Geophys. Res. 87 (C2), 1231–1238.
Ogburn, S.E., Loughlin, S.C., Calder, E.S., 2015. The association of lava dome growth with major explosive activity (VEI ≥ 4): DomeHaz, a global dataset. Bull. Volcanol. 77, 40.
Preece, K., Gertisser, R., Barclay, J., Charbonnier, S.J., Komorowski, J.-C., Herd, R.A., 2016. Transitions between explosive and effusive phases during the cataclysmic 2010 eruption of Merapi volcano, Java, Indonesia. Bull. Volcanol. 78, 54.
Pyle, D.M., 1989. The thickness, volume and grainsize of tephra fall deposits. Bull. Volcanol. 51, 1–15.
Saucedo, R., Macias, J.L., Gavilanes, J.C., Arce, J.L., Komorowski, J.C., Gardner, J.E., Valdez-Moreno, G., 2010. Eyewitness, stratigraphy, chemistry, and eruptive dynamics of the 1913 plinian eruption of Volcan de Colima, Mexico. J. Volcanol. Geotherm. Res. 191, 149–166.
Scott, W.E., Hoblitt, R.P., Torres, R.C., Self, S., Martinez, M.L., Nillos, T., 1996. Pyroclastic flows of the June 15 1991, climactic eruption, of Mount Pinatubo. In: Newhall, C.G., Punongbayan, R.S. (Eds.), Fire and Mud: Eruptions and Lahars of Mount Pinatubo, Philippines. University of Washington Press, pp. 545–570.
Sheridan, M.F., Barberi, F., Rosi, M., Santacroce, R., 1981. A model for Plinian eruptions of Vesuvius. Nature 289, 282–285.
Siebert, L., Simkin, T., Kimberly, P., 2011. Volcanoes of the World. third ed. University of California Press, Los Angeles, p. 551.
Sigurdsson, H., Carey, S.N., Fisher, R.V., 1987. The 1982 eruptions of El Chichon volcano, Mexico (3): physical properties of pyroclastic surges. Bull. Volcanol. 49, 467–488.
Sparks, R.S.J., 1997. Causes and consequences of pressurization in lava dome eruptions. Earth Planet. Sci. Lett. 150, 177–189.
Tanaka, H.L., Iguchi, M., Nakada, S., 2016. Numerical simulations of volcanic ash plume dispersal from Kelud volcano in Indonesia on February 13, 2014. J. Disaster Res. 11, 31–42.
Taylor, G.A.M., 1958. The 1951 eruption of Mount Lamington, Papua. Australia Bureau of Mineral Resources, Geology and Geophysics Bulletin 38, 129.
Valentine, G.A., 1998. Damage to structures by pyroclastic flows and surges, inferred from nuclear weapons effects. J. Volcanol. Geotherm. Res. 87, 117–140.
Walker, G.P.L., 1971. Grain-size characteristics of pyroclastic deposit. J. Geol. 79, 696–714.
Walker, G.P.L., 1973. Explosive volcanic eruptions – a new classification scheme. Geol. Rundsch. 62, 431–446.
Wilson, L., Huang, T.C., 1979. The influence of shape on the atmospheric settling velocity of volcanic ash particles. Earth Planet. Sci. Lett. 44, 311–324.
Wilson, L., Sparks, R.S.J., Walker, G.P.L., 1980. Explosive volcanic eruptions – IV. The control of magma properties and conduit geometry on eruption column behaviour. Geophys. J. R. Astron. Soc. 63, 117–148.
Wirakusumah, A.D., 1991. Some Studies of Volcano, Petrology and Structure of Mt. Kelut, East Java, Indonesia. PhD Thesis. Victoria University of Wellington, p. 460.
Woods, A.W., 1988. The fluid dynamics and thermodynamics of eruption columns. Bull. Volcanol. 50, 169–193.

Please cite this article as: Maeno, F., et al., A sequence of a plinian eruption preceded by dome destruction at Kelud volcano, Indonesia, on February 13, 2014, revealed from tep..., J. Volcanol. Geotherm. Res. (2018), http://dx.doi.org/10.1016/j.jvolgeores.2017.03.002